Elsevier Editorial System(tm) for Journal of Volcanology and Geothermal Research
Manuscript Draft

Manuscript Number: VOLGEO3718R1

Title: Triggering mechanisms of static stress on Mount Etna volcano. An application of the boundary element method.

Article Type: Research Paper

Keywords: Numerical modeling, Coulomb stress changes, volcano dynamics, Mount Etna volcano, magmatic activity.

Corresponding Author: Dr. Eugenio Privitera,

Corresponding Author's Institution: Istituto Nazionale di Geofisica e Vulcanologia

First Author: Eugenio Privitera

Order of Authors: Eugenio Privitera; Bonanno Amalia; Stefano Gresta; Giuseppe Nunnari; Giuseppe Puglisi

Abstract: In the last thirty years, numerous eruptions and associated deformation episodes have occurred at Mt. Etna volcano. Datasets recorded by continuous monitoring of these episodes provide a unique opportunity to study the relationships between volcanism, flank instability and faulting activity. We have investigated the stress triggering mechanism between magmatic reservoir inflation, intrusive episodes and flank dynamics. Using three-dimensional numerical Boundary Elements Models we simulated volcano-tectonic events and calculated Coulomb stress changes. Using this modeling approach, we analyzed four realistic scenarios that are representative of recent kinematics occurring at Mt. Etna. The main results obtained highlight how (1) the inflation of a deep spherical magma source transfers elastic stress to a sliding plane and faults (2) the opening of the NE Rift and S Rift (to a less efficient extent) favor movements of the instable sector and may encourage seismicity on the eastern flank faults, and (3) flank instability may trigger the uprising of magma. Defining the effects of the elastic stress transfer and relationships among the main forces acting on volcano, may help to forecast possible eruption scenarios during future episodes of unrest at Mount Etna and provide an important tool for decision makers during volcanic emergencies involving the highly populated areas of the volcano.

Triggering mechanisms of static stress on Mount Etna volcano. An application of the boundary element method.

E. Privitera[1], A. Bonanno[2], S. Gresta[1,3], G. Nunnari[2], G. Puglisi[1]*

1) Istituto Nazionale di Geofisica e Vulcanologia, Osservatorio Etneo, Piazza Roma 2, I-95123 Catania, Italy.
2) Università degli Studi di Catania, Dipartimento di Ingegneria Elettrica, Elettronica ed Informatica., Viale Andrea Doria 6, I-95125, Catania, Italy.
3) Università degli Studi di Catania, Dipartimento di Scienze Biologiche, Geologiche e Ambientali, Corso Italia 57, I-95129 Catania, Italy,

Running Title: Coulomb stress changes at Mount Etna

* Corresponding author:

Eugenio Privitera

Istituto Nazionale di Geofisica e Vulcanologia – Osservatorio Etneo

Piazza Roma 2, I-95123 Catania (Italy)

E-mail: eugenio.privitera@ct.ingv.it

Tel.: ++39 095 716 5844 – Fax ++39 095 716 5826

Abstract

In the last thirty years, numerous eruptions and associated deformation episodes have occurred at Mt. Etna volcano. Datasets recorded by continuous monitoring of these episodes provide a unique opportunity to study the relationships between volcanism, flank instability and faulting activity. We have investigated the stress triggering mechanism between magmatic reservoir inflation, intrusive episodes and flank dynamics. Using three-dimensional numerical Boundary Elements Models we simulated volcano-tectonic events and calculated Coulomb stress changes. Using this modeling approach, we analyzed four realistic scenarios that are representative of recent kinematics occurring at Mt. Etna. The main results obtained highlight how (1) the inflation of a deep spherical magma source transfers elastic stress to a sliding plane and faults (2) the opening of the NE Rift and S Rift (to a less efficient extent) favor movements of the instable sector and may encourage seismicity on the eastern flank faults, and (3) flank instability may trigger the uprising of magma. Defining the effects of the elastic stress transfer and relationships among the main forces acting on volcano, may help to forecast possible eruption scenarios during future episodes of unrest at Mount Etna and provide an important tool for decision makers during volcanic emergencies involving the highly populated areas of the volcano.

<u>Keywords</u>: Numerical modeling, Coulomb stress changes, volcano dynamics, Mount Etna volcano, magmatic activity.

1. Introduction

Active volcanoes in densely populated areas represent a primary hazard that requires a operative and well-timed interaction between research institutions and civil defence authorities during unrest episodes. Consequently, involved researcher are encouraged to tune up affordable methods that can provide realistic scenarios of the eruptive evolution in near real-time.

Mount Etna dynamics is the result of a complex interplay between magma ascent in the plumbing system, dike emplacement, tectonic uplift, faulting and flank instability. Many studies have highlighted that at Mount Etna increases in static stress induced by dike intrusions bring faults closer to failure (Gresta et al., 2005). More recently, the pressurization of a magmatic reservoir was considered to trigger 1997-1998 Mount Etna seismic swarms as a consequence of stress redistribution (Bonanno et al, 2011).

The increase in collected seismic and deformation measurements and the rapid growth of computational power have enabled improving investigations into the relationship between faulting, flank dynamics and magmatic activity using numerical modeling. Walter et al. (2005) modeled the 2002-2003 Mt. Etna eruption by means of Boundary Element Method, evaluating the influence of four different sources on the kinematics of the volcano’s eastern flank. They found a feedback relationship between flank movements and intrusive processes The numerical models suggest that magmatic activity (inflation of a reservoir and emplacement of dikes) encourages motion of the eastern flank, which, in turn, promotes magma to rise up to shallower levels within the volcano. Currenti et al. (2008) performed a Finite Element Modeling approach to evaluate ground deformation and the resulting stress redistributions in response to magmatic processes occurring during the 2002–2003 Etna eruption. They found that the changes in the state of stress generated by the southern dike produce an extensional stress field that favors magma propagation along the north-east Rift. The static stress changes computed onto the Timpe Fault System and the Pernicana Fault indicate that the magma intrusions on the southern and northeastern flanks prompted these seismogenic structures to slip.In this paper, we will use numerical simulations to hypothesize four realistic scenarios at Mt Etna in which one source at a time is active. Coulomb stress changes will be computed on three dimensional fault surfaces in order to investigate the interaction between intrusion/eruptive episodes, tectonic activity and flank instability. The method used requires a processing time of some tens of minutes and is thus suitable for a near real-time application in order to forecast the evolution of future unrest episodes.

2. Etna volcano setting

Mount Etna is a Quaternary basaltic stratovolcano located on the east coast of Sicily. It stands between two first-order tectonic elements: the Apenninic-Maghrebian Chain and the Hyblean Foreland (inset of Figure 1). The northern and western sectors of the volcano lie over metamorphic and sedimentary rocks belonging to the frontal nappes system of the Apenninic-Maghrebian Chain, whereas the southern and eastern sectors overlie marine clays of Quaternary age, deposited on the flexured margin of the northward-dipping downgoing Hyblean Foreland (Lentini, 1982) (inset of Figure 1).

Volcanic Activity

Recent volcanic activity of Mount Etna is characterized by eruptions at the four summit craters, and by fissure eruptions and dike intrusions at the rift zones oriented NE, south and west. During the last 400 years, about half of the eruptions occurred along the rift zones through fissures opened on the volcano flanks (Behncke and Neri, 2003). These fissures are usually related to the lateral intrusion of dikes radiating from a shallow magma conduit system.

Important results obtained during recent decades, mainly due to the rapid improvement in the seismic and deformation monitoring networks, have identified the main tectonic structures and the paths along which the magma rises beneath Mount Etna. Seismic tomographic images define the basement of Mount Etna as characterized by a main upper and middle crustal intrusion complex, with high V_p values (High Velocity Body; HVB), whose top is located at about 4 km below sea level (b.s.l), beneath the southeastern flank of Mount Etna (e.g., Aloisi et al., 2002; Chiarabba et al., 2004; Patanè et al., 2006). In recent years, magma intrusions have ascended along the western boundary of the HVB, as documented by ground deformation and seismic studies (e.g., Bonforte et al., 2008; Puglisi et al., 2008 and references therein). It is noteworthy that the lack of evidence for large magmatic storage volumes strongly supports the idea that, during its ascent along the western boundary of the HVB, the magma is stored as a plexus of dikes or sills, as suggested by Armienti et al. (1989) to justify the typical polybaric evolution of the magmas within the plumbing system of Mount Etna (Corsaro and Pompilio, 2004).

Structural framework

The shallow geodynamic behavior of Mount Etna seems to be controlled by the flank instability processes causing the seaward sliding of the volcano eastern side as a result of a complex interaction between regional tectonic stresses, gravity forces acting on the volcanic edifice and the dike-induced rifting (Neri et al., 1991; Borgia et al., 1992; Lo Giudice and Rasà, 1992; McGuire,1996; Rasà et al., 1996). Although the published models propose different explanations of the origin and depth of the flank movement, they all agree in identifying the Pernicana Fault system, PF (Figure 1) as the northern boundary of the unstable sector. This is a transtensive fault with left lateral movement. It is characterized by a high slip rate from 10 to 28 mm/year with shallow (<3.5 km) and moderate seismic activity (2<M<4.5) (Azzaro, 1997; Azzaro et al., 2001). The PF activity is kinematically connected to the episodic opening and eruptions of the nearby NE Rift (Figure 1) (Neri et al., 1991; Gardunõ et al., 1997; Tibaldi and Groppelli, 2002; Acocella and Neri, 2003; Acocella et al., 2003). The southern part of the western boundary of the unstable sector is represented by the South Rift (Rasà et al., 1996) joining, southeastward, with the Tremestieri-

Trecastagni fault system TTF (Figure 1). This fault system is made up of a number of NNW-SSE striking faults showing evident right-lateral displacement and is also characterized by very shallow seismicity, with typical focal depths of 1–2 km. Other tectonic lineaments dissect the southern and south-eastern sectors of the volcano, such as the Timpe Fault system (STF1 and STF2), San Leonardello Fault (SLF), Moscarello Fault (MF) and Santa Venerina Fault (SVF) (Figure 1).

Most of these faults have high sliprates from 1.0 to 2.7 mm/year (Azzaro, 2004; Puglisi et al., 2008), partly due to shallow seismicity (Lo Giudice and Rasa, 1992; Montalto et al., 1996). Instrumental data, according to historical and macroseismic information (Azzaro, 1999), indicate that more than 80% of earthquakes are shallower than 5 km (Gresta et al., 1990), which, despite their moderate magnitude, have often produced coseismic surface faulting. Fault plane solutions of these events frequently indicate a right lateral strike, combined with a significant normal component. More recent proposals emphasize the complexity of the unstable sector, showing how these faults represent the main structures that separate portions with slightly different velocities of downslope movement (Bonforte et al., 2011).

3. CFS Modeling

In this paper, we investigate the relationships between volcanism, flank instability and faulting in terms of elastic stress change. We investigate possible triggering conditions in which only one deformation source at a time is active. Our modeling approach examines how (1) the inflation of a spherical deep source interacts with the sliding plane and faults, (2) the opening of an eruptive fissure (at North-East or South Rift zone) affects the sliding movement of eastern sector or seismic activity on fault planes, (3) the flank instability governs the kinematics of faults and triggers (or inhibits) the ascent of magma (Figure 3).

3.1. Modeling Method

Taking into account the topographic effects, we compute boundary element solutions of deformation sources embedded in an elastic half-space, using the program Poly3D 2.1.8 (Thomas, 1993; Maerten et al., 2005). Based upon the boundary element method (Crouch and Starfield, 1983), Poly3D includes the fundamental solution to an angular dislocation in a homogeneous, linear elastic half-space (Comninou and Dundurs, 1975). A number of angular dislocations are juxtaposed to create polygonal boundary elements that collectively define discretized objects of arbitrary shape in three dimensions. Boundary conditions in Poly3D can be applied remotely (as constant stresses or strains), at the centers of each element of the discretized fault surface (as tractions or displacement), or as combinations. The program solves a series of linear algebraic equations that describe the influence of each element on every other element under a prescribed set of boundary conditions. Once the displacement distribution along a fault is determined, the static stress, strain and displacement fields around the fault are calculated using influence coefficient equations that relate the displacements at the fault to the resultant elastic field at any point in the surrounding linear elastic medium. This solution is superimposed upon the remote stress field boundary condition to produce the total elastic field. Note that in our modeling processes we do not take into account the regional stress field. Indeed, geological and geophysical evidences highlight the heterogeneity of the Mount Etna stress field in time and space (e.g., Barberi et al., 2000 and reference therein). According to Gresta et al. (2005), from a kinematic point of view, the coexistence of structural elements such as PF and TFS are incompatible with a homogeneous stress field. Consequently, in this paper we use only "Specified fault calculation" for ΔCFS computation and we relinquish the evaluation of ''optimally oriented faults'' (strongly influenced by the regional stress field) as suggested by several authors in such cases (e.g., Gresta et al. 2005, Bonanno et al., 2011 and references therein)

In Poly3D we build polygonal elements for modeling complex surfaces with curving boundaries. Surface fault changes in strike are meshed without gaps. The spherical void is built by assembling triangular, hexagonal or pentagonal elements in the same manner as a football.

The Boundary Element Method was chosen because it is suitable for near real-time applications since it allows modifying an evolving scenario simply by adding new magmatic sources and/or receiving structures. The use of Poly3D enables avoiding meshing the medium every time a structural modification is carried out, in such a way the computational time is limited to tens of minutes.

3.2. Setup of deformation source parameters

Following on from recent studies (Patanè et al., 2003a; Chiarabba et al., 2004; Bonaccorso et al., 2006; Bonforte et al., 2008; Puglisi et al., 2008;), we considered a spherical cavity constructed of 815 triangular elements, simulating a 1 km in radius reservoir at 3 km depth (Figure 2). An increase in magma pressure perturbs the stress field in the surrounding crust. Using positive traction boundary conditions, normal to the element, we defined a volume increase of $7.9*10^6$ m^3, a realistic value for inflating magma bodies (Bonaccorso et al., 2006; Palano et al., 2007; Puglisi et al., 2008). The center of the MR was located beneath the Summit Craters area (for details see Table 1). In addition, in order to evaluate the influence of depth of an inflating reservoir (hereafter MR) on other considered structures and in particular on SP, we performed two further simulations moving the center of the sphere by ± 2.4 km. These steps of depth were chosen since they roughly correspond to the projections respectively of the top and the bottom of SP (see below) along the vertical line intersecting the Summit Craters.

Dike intrusions were modeled by rectangular planes with a curving top boundary matching the topography (Figure 2). A uniform element-normal displacement discontinuity of 2.5 m is imposed on dikes. The geometry of the North-East and South dikes used in this paper is based on values published by Puglisi et al. (2008). In any case, openings larger than 3 m do not modify the results significantly. The parameters of the modeled dikes are reported in Table 1.

In agreement with inversion models inferred from ground deformation measurements (Puglisi and Bonforte, 2004; Bonaccorso et al., 2006; Bonforte et al., 2008), we modeled a sub-horizontal sliding plane (hereafter SP) as a rectangular surface 20 km long and 25 km wide, with a main normal (7.7 cm) and minor dextral component (4.4 cm) (Figure 2). Although the slip amount depends on the period investigated, inversion models published (Puglisi and Bonforte, 2004; Palano et al, 2007) found an overall sliding in the range of 4 – 9 cm/year in the period 1993 -2000.

3.3. Setup of topography and fault parameters

We used the Global Digital Elevation Model (INGV-G-DEM) that merges inland DEM (Tarquini et al., 2007; Neri et al., 2008) and bathymetric data sets available for the Mount Etna area (Bosman et al., 2007; Cavallaro et al., 2008). The original data were integrated and interpolated, becoming homogenous with a final resolution of 10 m pixel size. Using INGV-G-DEM resampled with a resolution of 100 m, we built a rectangular surface of 3500 km^2 (extending for about 70 kilometers in longitude and 50 km in latitude) and discretized with 3184 triangular meshes (Figure 2). Volcano topography is assumed as a traction-free surface in order to study the influence on displacements and stress numerical calculations. According to geological and structural studies integrated with seismic data, we modeled the main tectonic lineaments of the eastern sector of the volcano. We built the faulting planes as rectangular surfaces with a curving top boundary matching the topography, with each plane discretized by triangular meshes with a mean areal dimension of about 0.027 km^2. In particular, Provenzana Fault (PR) shows a change of strike from N35°E to N55°E, thus a curving top boundary is modeled. The Pernicana Fault (PF) is made up of four segments (PF1, PF2, PF3 and PF4) striking N88°E, N102°E, N114°E, N120°E, respectively (Figure 2a). The southern border of the unstable sector is represented by the Tremestieri-Trecastagni Fault system (TTF) modeled with a sub-vertical plane with a sharp change in direction (from N103°E to N150°E). The Timpe Fault System is made up of two segments, STF1 and STF2, with strike direction N165°E and N3°W, respectively. These latter fault systems, together with SLF, MF, SVF, all striking from N173°E to N140°E, reach the depth of the sliding plane (see Figure 2b). The sub-vertical fault planes above the sliding plane (SP) have a width ranging from 1950 to 2800 m (for details see Table 2). In our models, we assume that receiver faults are discontinuities embedded in an elastic half-space in which they are free to move in any direction.

3.4 Coulomb Stress Changes

We calculated Coulomb stress changes caused by volcanic sources on modeled fault planes, while computing changes in volumetric or normal stress near the magma chamber or eruptive dikes caused by flank movements or earthquakes (e.g. Savage and Clark 1982; Nostro *et al.* 1998; Toda *et al.* 2002). It is widely accepted that static stress changes ($\geq$ 0.1 bars) induced by a magmatic source may trigger seismicity within a rock volume close to the critical state of failure (e.g., Reasenberg and Simpson, 1992; Stein, 1999). Spatial and temporal relationships between stress changes and earthquakes are explained through the Coulomb failure stress change, defined as:

$$\Delta CFS = \Delta\tau + \mu(\Delta\sigma_n + \Delta P) \qquad (1)$$

where $\Delta\tau$ is the shear stress change computed in the direction of slip on the fault, $\Delta\sigma_n$ is the normal stress change (positive for extension), μ is the coefficient of friction and ΔP is the pore pressure change (e.g., King *et al.*, 1994; Harris, 1998; King and Cocco, 2000). For simplicity, we considered here a constant effective friction model (Beeler *et al.*, 2000; Cocco and Rice 2002) that assumes ΔP is proportional to the normal stress changes ($\Delta P = -B\Delta\sigma_n$, where B is the Skempton parameter):

$$\Delta CFS = \Delta\tau + \mu'\Delta\sigma_n \qquad (2)$$

where μ' is the effective friction ($\mu' = \mu[1 - B)]$). The fault is brought closer to failure when ΔCFS is positive. In order to verify if dike intrusions or magmatic reservoir inflations are encouraged, we evaluate the change of the volumetric strain ($\Delta\varepsilon = \varepsilon_1 + \varepsilon_2 + \varepsilon_3$) on the magmatic reservoir and horizontal normal stress changes ($\sigma_m = \Delta\sigma_{xx} + \Delta\sigma_{yy}) / 2$) on the rift zone dikes. Indeed, the unclamping of a rift zone ($\sigma_m > 0$) induced by fault dislocations may facilitate the ascent of new magma and dike injection. In the same way, the unclamping may favor the decompression of the magma reservoir, leading to the formation and ascent of bubbles and then increasing the magma overpressure. We performed all calculations in a homogeneous Poissonian elastic half-space using a Poisson ration of $\nu = 0.25$ and a Young modulus of E = 75 GPa, and a $\mu' = 0.4$.

3.5 Assumptions of numerical modeling

Coulomb stress changes are evaluated in a homogenous elastic half-space. Thus mechanical heterogeneities, for instance due to thermal structure, a hydrothermal altered volcanic core or a mechanically rigid basement, are not taken into account by our models. As stated before, the regional stress field is not taken into account given its heterogeneity in space and time. The surface traces of the faults are visible, well-mapped and constrained, but we simplified the characteristics of the sliding plane by imposing a uniform slip on the whole rectangular surface. We did not take into account visco-elastic or elasto-plastic behaviors or any differential flank movement inferred by a number of authors recently (Palano et al., 2009; Currenti et. al, 2010;Bonforte et al., 2011).

4. Modeling

For each model, ΔCFS values are computed on faulting planes and on the sliding surface (Figure 2). The normal stress σ_m is evaluated on dike fractures and volumetric strain $\Delta\varepsilon$ on the spherical surface of magmatic reservoir. The parameters of sources and receiver structures are described in Table 1 and 2, respectively. Four deformation models were tested: M1, inflating of a spherical magmatic source (Figure 3, M1); M2, opening of eruptive fissures (Figure 3, M2), divided into two models A) for South dike and B) North East dike; and M3, sliding of planar surface (Figure 3, M3). Our numerical results of ΔCFS on each receiver structures are reported in Tables 3-6.

4.1. Model 1 - Mogi Source

a) Stress calculations

We first considered stress changes associated with a reservoir inflation (depth = 3.0 km, roughly coincident with the center of the SP). M1 shows a decrease of CFS along the PR and PF2 segments and an increase along the PF1 segment, with the latter showing a maximum value of 1.4 bars along the western edge (see M1 in Figure 4 and Table 3 for maximum and minimum ΔCFS values). A decrease and an increase close to zero were computed on PF3 and PF4 planes, respectively (Table 3). M1 induces a stress increment on STF1 and SVF closer portions (0.3 and 0.2 bars). The MF, SLF and TTF planes are subjected to a slight positive increment on the top edge (in a range between 0.1 and 0.2 bars) (Figure 4, M1). Moreover, the movement of STF2 is inhibited by the inflation of MR. Finally, the inflation of spherical chamber favors the closure of the NE and South dikes significantly. On the sliding plane, we observed a decrease of ΔCFS in the northwestern part of the plane (minimum value about -2 bars) and a very slight positive variation (0.2 bars) along the remaining part of the surface.

The simulations performed moving the depth of MR do not change the scenario described before drastically and significant variations only affect a few structures. A shallow MR (depth = 0.6 km; roughly coincident with the top boundary of the SP) does not change the pattern of the static stress on all the faults considered, and the intensity is only slightly affected. Also the NE dike shows almost unaltered features and only a very small part of the dike (near MR) underwent an unclamping effect. The most important variation is observed on the SP, which experienced a positive CFS variation of 2 bars. The S dike also showed a different pattern in ΔCFS distribution; indeed, the closure of the S dike is strongly encouraged only in the portion near MR, while the remaining part underwent an unclamping effect. The inflation of a deeper MR (depth = 5.4 km; roughly coincident with bottom boundary of the SP) does not change the static stress pattern on the SP and the S and NE dikes. A slight change in the intensity affected both dikes, enhancing the closure trend observed with a 3 km depth MR. Also the majority of the faults considered show unchanged features and only MF experienced a positive CFS variation until 1.4 bars.

In summary, the depth of an inflating shallow crustal reservoir may change the scenario evaluated slightly and only the flank movement seems significantly affected by the depth of MR; indeed, very shallow MR may promote flank movements, while deeper MR inhibits them. In general, a shallow MR discourages dike intrusion into the Mount Etna rift zones and promotes the stress triggering on the westernmost portion of PF.

b) Displacement calculations

The expansion of MR at 3 km depth induced the uplift of the nearby structures, such as PR, PF1 and PF2 (see Figure 5 and Table 3 for maximum and minimum displacement values). The inverse component is replaced by left-lateral movement on PF3 and PF4 components. The displacement values are progressively reduced from the western to eastern part. SLF, STF2, TTF and MF shows a right-lateral movement. On STF1, SVF and SP planes an uplift is favored. In particular, on the SP a maximum value of 2.4 centimeters of thrust movement is computed. This result changes drastically if we consider a very shallow crustal reservoir, which inverts the observed trend, promoting seaward movements of the eastern flank. It is clear that for this aspect of the problem the boundary condition set in the model (source depth) plays a basic role and highlights just how crucial the depth constraint is in ground deformation inversion analyses.

4.2. Model 2A – South Dike

a) Stress calculations

Intrusion along the S dike favors the closure of NE dike with a negative unclamping effect (σ_m maximum value is about of -32 bars). In the M2a we observe a decrease of ΔCFS on the PR segment (max value -4.5 bars). On the PF system ΔCFS values are negative except on PF1 with a positive stress variation reaching a maximum value of 1.4 bar on the upper part of plane (Table 4). PF2, PF3, PF4 and SLF segments show a slight increase but in general all planes show a reduction of ΔCFS. STF1, STF2, SVF and TTF similarly underwent a reduction of ΔCFS (see M2A in Figure 4 and Table 4 for maximum and minimum ΔCFS values). On SP a maximum positive stress change is computed for the part of the plane closest to the magmatic feeding system. Finally, the S-dike intrusion induces a compression ($\varepsilon>0$) on the MR located beneath the summit craters (see Figure 4, M2A).

b) Displacement calculations

The opening of SD encourages a normal movement of SP. The direction of displacement vectors on SVF, SLF, STF1, STF2 and MF shows a right-lateral movement associated with the dip-normal component. PR and TTF segments show the reverse movement. All PF segments move with a pure left-lateral strike slip (see Figure 5 and Table 4 for maximum and minimum displacement values). In summary, magmatic activity in the South Rift closes the North East Rift and mobilizes the East and North East region of the unstable block.

4.3. Model 2B – North East Dike

a) Stress change calculations

In M2B we find that intrusion along the NE dike into the rift zones causes significant increase of ΔCFS on PR and PF1, with maximum values of about 320 bars and 100 bars, respectively. On the upper part of PF2 elastic stress changes increase to 3.4 bars. PF3, STF1, SVF, STF2 and TTF show a decrease of static stress variations (Table 5). SLF and MF are brought close to failure on the shallower portions of fault planes with higher values of 2.3 and 5.3 bars, respectively (see M2B in Figure 4 and Table 5 for maximum and minimum ΔCFS values). A significant negative unclamping effect on the walls of the S dike is found (max σ_m value about of -26 bars). The opening of the NE dike favors the decompression of MR with ε_{max} about of -4.8e-5 m^3($\varepsilon<0$ volumetric strain is negative for decompression). Finally, we observe that because of its dimension and geometry, the

NE dike is more efficient in transferring stress on the sliding plane with respect to the S dike. On the shallower portion of SP the maximum value of ΔCFS reaches 2.6 bars (Table 5).

b) Displacement calculations

The most important results regarding displacement calculations show that the opening of the NE dike favors the sliding of flank with a transtensive component (see Figure 5 and Table 5 for maximum and minimum displacement values). All modeled faults, such as TTF, SVF, STF1, STF2, MF and STF are kinematically compatible with a right-lateral movement associated with a normal dip component. On PR, PF1 and PF2 planes a transpressive left-lateral movement is favored. Towards the east we found only left transcurrent component on PF3 and PF4 structures.

4.4. Model 3 – Sliding Plane

a) Stress calculations

We found a positive ΔCFS with max values of about 1.7 and 1.5 bars in the upper part of PF1 and PF2, respectively, and an increase of static stress in the lower portion of PF3 and PF4 (max about of 3.5 bars). The relative position between SP and receiver faults also resulted in an increase in static stress on TTF plane. Thus, we estimated a positive ΔCFS in the lower part of this structure with a maximum value of 3 bars (see M3 in Figure 4 and Table 6 for maximum and minimum ΔCFS values). Small increases of elastic stress are found on the MF, SLF, SVF, STF1 and SFT2 faults (Table 6). The sliding of the plane beneath the eastern flank seems to favor a compression for MR ($\varepsilon>0$ volumetric strain is positive). The unclamping effects for two vertical eruptive fractures located on the northeast and southern flank of volcano was estimated. We observed that SP induces the closure in the upper part of tabular dikes. Instead, a small opening is favored in their deeper zones (about 0.1 bars) (Figure 4, M3). This interaction depends on the dimension of modeled eruptive fractures and the depth of SP. In brief, the unstable condition of flank sliding toward the sea may affect the magmatic system. Decompression of plumbing system may lead to the ascent of new magma or modify the condition of overpressure with the formation of bubbles (Hill, 2002).

b) Displacement calculations

The results of our simulations (see Figure 5 and Table 6 for maximum and minimum displacement values) show that the transtensive movement of SP encourages the dip normal displacement on PR, PF1 and PF2. By contrast, PF3 and PF4 moves according to a dip-normal associated to a left lateral movement. Coherently to observed kinematics STF1, STF2, SLF, SVF and MF are encouraged to move with a transtensive component, whereas a transpressive movement is determined for TTF.

5. Discussion and conclusions

During these last decades Mount Etna volcano has undergone several eruptions that have highlighted intriguing trigger mechanisms and have featured dike intrusions, activation of seismogenic faults and aseismic ground deformations.

Geophysical studies suggest that complex dynamics, involving more than one source (seismogenic sources and dikes), is a relatively common characteristic of eruptive episodes on Mount Etna. Gresta et al. (2005), for instance, highlighted that earthquakes along the PF and STF were induced by the static stress variations associated with the emplacement of eruptive dikes during the 1981 and 2001 eruptions, respectively. More recently, the pressure increase due to magma ascent episodes occurring in 1997-1998 at Mount Etna has been demonstrated to be responsible for the reactivation of seismogenic structures on the western side of the volcano (Bonanno et al., 2011). In Bonanno et al. (2011), the intrusive process was modelled as an inflating Mogi source located at 5.5 km depth, but in the present work, we emphasize the crucial role of the boundary condition set in the model (source depth) and show the possible scenarios with a shallower MR depth (Model M1).

The July-August 2001 eruption was characterized by a very complex field of flank eruptive fractures located largely on the upper southern slope of the volcano (Monaco et al., 2005). The eruption onset was preceded and accompanied by significant earthquakes (Patanè et al., 2003b) and marked ground deformations (Bonaccorso et al., 2002). The main source of deformations was modelled by a tensile dislocation located on the South Rift zone (Puglisi et al. 2008) as also confirmed by the Seismic Moment Tensor inversions of the best constrained earthquakes that heralded the opening of the eruptive fractures (Saraò et al., 2010). Our present model M2A takes account of the main behaviour of the magmatic source for this eruption well.

The October 2002 - January 2003 eruption occurred on two sides of the volcano, along the upper north-eastern (NE Rift zone) and southern (South Rift Zone) flanks. Once again, earthquakes and ground deformations preceded and accompanied the opening of the eruptive fractures (Barberi et al., 2004 and reference there in). The two intrusive dikes have been satisfactorily modelled by two separate tensile dislocations (Aloisi et al., 2003). During the first stage of the eruption, several seismogenic structures on the eastern flank became successively active. This was explained as due to the transfer of elastic stress from the magmatic source to faults (PR and PF) and afterwards from faults to faults (Barberi et al., 2004). Our present model M2B is schematically representative of the first stage of the above cited domino effect phenomena.

Finally, the 2004–2005 eruption emitted a highly degassed magma from a sub-terminal fracture. During the first weeks of activity, the erupted magma was already residing inside the volcano, probably since the 2002-2003 eruption, while later it mixed with new magma ascending through the central conduit system (Corsaro et al., 2009). Magma intruded passively due to the exceptional extension on the summit area caused by the large sliding of the eastern flank of the volcano (almost 9 cm of slip; Bonaccorso et al., 2006). The east flank sliding toward the sea induces a decompression on the shallow magma plumbing system as foreseen by our model M3 that simulates the unstable condition of this sector.

In this work we have investigated, by using the Boundary Element Method, how (*i*) the inflating of a deep spherical source interacts with a sliding plane and with faults and rift elements; (*ii*) the opening of eruptive fissures affects the sliding movement of the eastern sector of Mount Etna, encouraging earthquakes on fault planes; and (*iii*) the instability of the eastern flank governs the kinematics of faults and/or triggers the ascent of magma. The results presented here are strongly dependent on all the assumptions made. In particular, the lack of seismological constraints (hypocenter patterns and compatible fault plane solutions) for the sliding plane induced us to simplify the geometry of a detachment volume that remains/lies at the base of the instable sector. Nevertheless, our numerical results show good agreement with deformation measurements that well-describe the eastern flank dynamics of Etna volcano (e.g., Bonforte et al., 2008; Puglisi et al., 2008).

The main results obtained are the following:

1. The inflation of a magma reservoir encourages the slip on the westernmost segment of the Pernicana fault (PF).
2. The depth of MR is crucial, very shallow depth MR promote seaward movement of the eastern flank, while deeper MR (3.0 - 5.5 km) inhibit the movement.
3. Dikes intruding either on the NE or/and South Rift Zones favor the sliding of the planar source in its upper part and along the westernmost of PF.
4. The intrusion (opening) of a South dike favors the closure of a NE dike, while at the same time the opening of NE tensile fracture inhibits the ascent of magma along the South zone.
5. The intrusion of a NE dike (for dimension and kinematics) favors the Eastern flank sliding, more than the opening of an S dike.
6. The opening of a NE dike encourages the decompression of the magma plumbing system (depth = 3.0 km), evaluated by a high negative value of volumetric strain.
7. The passive sliding of SP promotes an increase of CFS on the westernmost and the central segments of PF. Its easternmost segments are brought close to failure at their bases.

8. The unstable condition of flank sliding toward the sea may affect the magmatic system and decompression of plumbing system may lead to a new magma ascent.
9. The western part of Pernicana fault (PF1) experienced a positive CFS for all the scenarios hypothesized. The other segments underwent a positive stress variation only in M2B and M3. In particular, Model M2B highlights the governing role of the intrusion in the NE Rift on the dynamics of this structure and on the dynamics of the Provenzana fault too.
10. Other faults considered seem to be less sensitive to the stress variation induced by sources considered, with the exception of three structures. SLF and MF underwent a significant positive CFS variation in model M2B, and TTF experienced an increase in static stress in model M3.

These results schematically represent possible scenarios of the evolution of the kinematic "activity" of Mount Etna volcano. The three basic elements (magma dynamics, earthquake occurrence and flank instability) interact with each other, alternating their active or passive role in a broader combination of domino effects. Our results are in general agreement with the findings of Walter et al. (2005), despite the significant differences in the structural setup and in the definition of geometrical characteristics of the single geological objects. The main difference regards the effect of interaction between magma reservoir and sliding plane; the latter was defined by Walter et al. (2005) with geometrical characteristics that are entirely different from those hypothesized in this paper. Currenti et al. (2008) use a very simplified structural setup taking into account only the two rift zones and the main fault systems in eastern flank. Regardless of differences, the result obtained are similar with the exception of the NE dike response to an intrusion in the South rift. Currenti et al. (2008) have also demonstrated that the introduction of an heterogeneous medium induces variation in the intensity of ΔCFS (as a function of modelled elastic parameters), but does not distort the geometrical pattern. The authors also show how the stress shape is affected by Mt. Etna topography. The main discrepancies are largely restricted to the volcano summit area because of the accentuated topography.

We note that the strength of our approach lies in the fact that we evaluate the distribution of the CFS pattern while taking into account the relevant effects of topography. In addition, we use a method that requires a processing time of some tens of minutes. It allows modifying an evolving erupting scenario simply by adding or alterating magmatic sources and/or receiving structures without needing any further computational time that other numerical methods require (e.g., re-mesh of medium in Finite Element Method). The real-time seismic and geodetic networks currently operating on Mount Etna are able to provide good enough data (both in number and quality) to satisfactorily (and rapidly) constrain the source(s) responsible for volcanic unrest. The application of the Boundary Element Method during volcanic unrest appears a promising tool to provide some possible scenarios of evolving volcanic activity in near real-time in terms of flank sliding and/or activation of either (both) seismogenic faults and/or magma bodies.

Acknowledgments

This work was funded by the INGV-DPC project V4_Flank. We thank Stephen Conway for correcting and improving the English. Amalia Bonanno was supported by INGV-DPC fellowships.

We thank the editor Joan Marti and two anonymous reviewers for the careful revision that enabled improving the paper significantly. The DEM used in this paper is the result of the integration of data available at INGV, in particular the DEM_ Sicilia 1999 (Tarquini et al., 2007) and the DEM_Lidar 2005 (Neri et al., 2008). This DEM was produced in the framework of the ASI-SRV project, and INGV-DPC V4-Flank project, thanks to Dr. F. Guglielmino (INGV, Osservatorio Etneo).

References

Acocella, V., Neri, M., 2003. What makes flank eruptions? The 2001 Mount Etna eruption and its possible triggering mechanisms. Bull. Volcanol. 65, 517–529.

Acocella, V., Behncke, B., Neri, M., D'Amico, S., 2003. Link between major flank slip and 2002-2003 eruption at Mount Etna (Italy). Geophys. Res. Lett. 30(24), 2286. doi:10.1029/2003GL018642.

Aloisi, M., Cocina, O., Neri, G., Orecchio, B., Privitera, E., 2002. Seismic tomography of the crust underneath the Etna volcano, Sicily. Phys. Earth Planet. In. 134, 139–155.

Aloisi, M., Bonaccorso, A., Gambino, S., Mattia, M., Puglisi, G., 2003. Etna 2002 eruption imaged from continuous tilt and GPS data., Geophys. Res. Lett. 30(23), 2214. doi:10.1029/2003GL018896.

Armienti, P., Innocenti, F., Petrini, R., Pompilio, M., Villari, L., 1989. Petrology and Sr-Nd isotope geochemistry of recent lavas from Mt. Etna: Bearing on the volcano feeding system. J. Volcanol. Geotherm. Res. 39, 315– 327. doi:10.1016/0377-0273(89)90095-4.

Azzaro, R., 1997. Seismicity and active tectonics along the Pernicana fault, Mt. Etna (Italy). Acta Vulcanol. 9, 7-14.

Azzaro, R., 1999. Earthquake surface faulting at Mount Etna volcano (Sicily) and implications for active tectonics. *J. Geodynamics* 28, 193-213. doi:10.1016/S0264-3707(98)00037-4.

Azzaro, R., 2004. Seismicity and active tectonics in the Etna region: Constraints for a seismotectonic model. In: Bonaccorso, A, et al. (Eds.), Etna Volcano Laboratory. Geophys. Monogr. Ser., vol. 143, AGU, Washington, D. C., pp. 205–220.

Azzaro, R., Mattia, M., Puglisi, G., 2001: Fault creep and kinematics of the eastern segment of the Pernicana Fault (Mt. Etna, Italy) derived from geodetic observations and their tectonic significance. Tectonoph., 333, 3/4, 401-415.

Barberi, G., Cocina, O., Neri, G., Privitera, E., Spampinato, S., 2000. Volcanological inferences from seismic straintensor computations at Mt. Etna Volcano, Sicily. Bull. Volcanol. 62, 318– 330.

Barberi, G., Cocina, O., Maiolino, V., Musumeci, C., Privitera, E., 2004. Insight into Mt. Etna (Italy) kinematics during the 2002–2003 eruption as inferred from seismic stress and strain tensors. Gephys. Res. Lett. 31, L21614. doi:10.1029/2004GL020918.

Beeler, N.M., Simpson, R.W., Lockner, D.A., Hickman, S.H., 2000. Pore fluid pressure, apparent friction and Coulomb failure. J. Geophys. Res. 105, 25533– 25554.

Behncke, B., Neri, M., 2003. Cycles and trends in the recent eruptive behaviour of Mount Etna (Italy). Can. J. Earth Sci. 40, 1405 – 1411. doi:10.1139/E03-052.

Bonaccorso, A., Aloisi, M., Mattia, M., 2002. Dike emplacement forerunning the Etna July 2001 eruption modeled through continuous tilt and GPS data. Geophys. Res. Lett. 29 (2), 1–4. doi: 10.1029/2001GL014397.

Bonaccorso, A., Bonforte, A., Guglielmino, F., Palano, M., Puglisi, G., 2006. Composite ground deformation pattern forerunning the 2004– 2005 Mount Etna eruption. J. Geophys. Res. 111, B12207. doi:10.1029/ 2005JB004206.

Bonanno, A., Palano, M., Privitera, E., Gresta, S., Puglisi, G., 2011. Magma intrusion mechanisms and redistribution of seismogenic stress at Mt. Etna volcano (1997-1998). Terra Nova 23, 339-348. doi: 10.1111/j.1365-3121.2011.01019.x.

Bonforte, A., Bonaccorso, A., Guglielmino, F., Palano, M., Puglisi, G., 2008. Feeding system and magma storage beneath Mt. Etna as revealed by recent inflation/deflation cycles. J. Geophys. Res. 113, B05406. doi:10.1029/2007JB005334.

Bonforte, A., Guglielmino, F., Coltelli, M., Ferretti, A., Puglisi, G., 2011. Structural assessment of Mount Etna volcano from Permanent Scatterers analysis. Geochem. Geophys. Geosyst. 12, Q02002. doi:10.1029/2010GC003213.

Borgia, A., Ferrari, L., Pasquarè, G., 1992. Importance of gravitational spreading in the tectonic and volcanic evolution of Mount Etna. Nature 357, 231– 235. doi:10.1038/357231a0.

Bosman A., Cavallaro, D., Chiocci, F.L., Coltelli, M., 2007. New insights on the Etna offshore reveal unknown morphological features related to the volcano eastern flank dynamics. Geoitalia 2007- Sesto Forum Italiano di Scienze della Terra. Rimini, 12-14 settembre 2007. ISSN 1972-1552 pp. 117.

Cavallaro D., Lodi, M., Bosman, A., Chiocci F., Coltelli, M., 2008. Evidenze di faglie attive nell'offshore etneo rilevate da analisi morfos strutturali. Riassunti del 84° Congresso Nazionale Società Geologica Italiana 3/3, pp. 204-205. (in Italian)

Chiarabba, C., De Gori, P., Patanè, D., 2004. The Mt. Etna plumbing system: The contribution of seismic tomography. In: Bonaccorso, A, et al. (Eds.), Etna Volcano Laboratory. Geophys. Monogr. Ser., vol. 143, , AGU, Washington, D. C., pp. 191– 204.

Cocco, M., Rice, J., 2002. Pore pressure and poroelasticity effects in Coulomb stress analysis of earthquake interactions. J. Geophys. Res. 107. doi:10.1029/2000JB000138.

Corsaro, R.A., Pompilio, M., 2004. Dynamics of magmas at Mount Etna. In: Bonaccorso, A, et al. (Eds.), Etna Volcano Laboratory. Geophys. Monogr. Ser., vol. 143, AGU, Washington, D. C., pp. 91– 110.

Corsaro, R.A., Civetta, L., Di Renzo, B., Miraglia, L., 2009. Petrology of lavas from the 2004-2005 flank eruption of Mt. Etna, Italy: inferences on the dynamics of magma in the shallow plumbing sysyem. Bull. Volcanol. 71, 781-793, doi:10.1007/s00445-009-0264-z.

Comninou, M. A., Dundurs, J., 1975. The angular dislocation in a half-space. J. Elasticity 5, 203–216.

Crouch, S.L., Starfield, A.M., 1983. Boundary Element Methods in Solid Mechanics: With Applications in Rock Mechanics and Geological Engineering. Allen and Unwin, St. Leonards, N.S.W., Australia.

Currenti, G., Del Negro, C., Ganci, G., Williams, C. A., 2008., Static stress changes induced by the magmatic intrusions during the 2002–2003 Etna eruption. J. Geophys. Res. 113, B10206, doi:10.1029/2007JB005301.

Currenti, G., Bonaccorso, A., Del Negro, C., Scandura, D., Boschi, E., 2010. Elasto-plastic modeling of volcano ground deformation. Earth and Planetary Science Letters 296, 311–318.

Gardunõ, V.H., Neri, M., Pasquarè, G., Borgia, A., Tibaldi, A., 1997. Geology of NE-Rift of Mount Etna, Sicily (Italy). Acta Vulcanol. 9(1/2), 91– 100.

Gresta, S., Longo, V., Viavattene, A., 1990. Geodynamic behaviour of eastern and western sides of Mt. Etna. Tectonophysics 179, 81 – 92. doi:10.1016/0040-1951(90)90357-E.

Gresta, S., Ghisetti, F., Privitera, E., Bonanno A., 2005. Coupling of eruptions and earthquakes at Mt. Etna (Sicily, Italy): A case study from the 1981 and 2001 events. Geophys. Res. Lett. 32. doi:10.1029/ 2004GL021479.

Harris, R.A., 1998. Introduction to special section: Stress triggers, stress shadows, and implications for seismic hazard. J. Geophys. Res. 103, 347–24.

Hill, D.P., Pollitz, F., Newhall, C., 2002. Earthquake-volcano interactions Phys. Today 55(11), 41–47.

King, G.C.P., Stein, R.S., Lin, J., 1994. Static stress changes and the triggering of earthquakes Bull. Seismol. Soc. Am. 84, 935– 953.

King, G.C.P., Cocco, M., 2000. Fault interaction by elastic stress changes: new clues from earthquake sequences. Adv. Geophys.44, 1–38.

Lentini, F., 1982. The geology of the Mt. Etna basement. Mem. Soc. Geol. Ital. 23, 7 –25.

Lo Giudice, E., Rasà, R., 1992 Very shallow earthquakes and brittle deformation in active volcanic areas: The Etnean region as an example. Tectonophysics 202, 257– 268.

Maerten, F., Resor, P., Pollard, D., Maerten, L., 2005. Inverting for slip on three-dimensional fault surfaces using angular dislocations. Bull. Seism. Soc. Am. 95, 1654–1665. doi:10.1785/0120030181

McGuire, W.J., 1996 Volcano instability: A reviewof contemporary themes. In: McGuire, W.M., Jones, A.P., Neuberg, J., (Eds.), Volcano Instability on the Earth and Other Planets. Geol. Soc. Spec. Publ., Geological Society (London) Special Publications 110, pp. 1– 23.

Monaco, C., Catalano, S., Cocina, O., De Guidi, G., Ferlito, C., Gresta, S., Musumeci, C., Tortorici, L., 2005. Tectonic control on the eruptive dynamics at Mt. Etna volcano (eastern Sicily) during the 2001 and 2002-2003 eruptions. *J. Volcanol. Geotherm. Res*. 144, 211-233.

Montalto, A., Vinciguerra, S., Menza, S., Patanè, G., 1996. Recent seismicity of Mount Etna: implications for flank instability, In: McGuire, W.J., Jones, A.P., Neuberg, J., (Eds.), Volcano instability on the Earth and other planets. Geological Society (London) Special Publications 110, pp. 169-177.

Neri, M., Gardunõ, V.H., Pasquarè, G., Rasà, R., 1991. Studio strutturale e modello cinematico della Valle del Bove e del settore nord-orientale etneo. Acta Vulcanol. 1, 17– 24. (in Italian)

Neri, M., Mazzarini, F., Tarquini, S., Bisson, M., Isola, I., Behncke, B., Pareschi, M.T., 2008. The changing face of Mount Etna's summit area documented with Lidar technology Geophys. Res. Lett. 35, doi:10.1029/2008GL033740.

Nostro, C., Stein, R.S., Cocco, M., Belardinelli, M.E., Marzocchi, W., 1998. Two-way coupling between Vesuvius eruptions and southern Apennine earthquakes, Italy, by elastic stress transfer. J. Geophys. Res. 103, 24487– 24504.

Patanè, D., De Gori, P., Chiarabba, C., Bonaccorso, A., 2003a. Magma ascent and the pressurization of Mount Etna's volcanic system. Science 299, 2061– 2063.

Patanè, D., Privitera, E., Gresta, S., Akinci, A., Alparone, S., Barberi, G., Chiaraluce, L., Cocina, O., D'Amico, S., De Gori, P., Di Grazia, G., Falsaperla, S., Ferrari, F., Gambino, S., Giampiccolo, E., Langer, H., Maiolino, E., Moretti, M., Mostaccio, A., Musumeci, C., Piccinini, D., Reitano, D., Scarfì, L., Spampinato, S., Ursino, A., Zuccarello, L., 2003b. Seismological constrains for the dike emplacement of the July-August 2001 lateral eruption at Mt. Etna volcano, Italy. *Ann. Geophys*. 46, 599-608.

Patanè, D., Barberi, G., Cocina, O., De Gori, P., Chiarabba, C., 2006. Time-resolved seismic tomography detects magma intrusions at Mount Etna, Science 313**,** 821–823.

Palano, M., Puglisi, G., Gresta, S., 2007. Ground deformation at Mt. Etna: a joint interpretation of GPS and InSAR data from 1993 to 2000. Boll. Geofis. Teor. Appl. 48, 81–98.

Palano, M., Gresta, S., Puglisi, G., 2009. Time-dependent deformation of the eastern flank of Mt. Etna: after-slip or viscoelastic relaxation? Tectonophysics 473, 300-311. doi:10.1016/j.tecto.2009.02.047.

Puglisi, G., Bonforte, A., 2004. Dynamics of Mount Etna Volcano inferred from static and kinematic GPS measurements. J. Geophys. Res. 109, B11404, doi:10.1029/2003JB002878.

Puglisi, G., Bonforte, A., Ferretti, A., Guglielmino, F., Palano, M., Prati, C., 2008. Dynamics of Mount Etna before, during, and after the July–August 2001 eruption inferred from GPS and differential synthetic aperture radar interferometry data. J. Geophys. Res. 113. doi:10.1029/2006JB004811.

Rasà, R., Azzaro, R., Leonardi, O., 1996. Aseismic creep on faults and flank instability at Mt. Etna volcano. In: McGuire, W.J., Jones, A.P., Neuberg, J., (Eds.), Volcano instability on the Earth and other planets. Geological Society (London) Special Publications 110, pp. 179– 192.

Reasenberg, P.A., Simpson, R.W., 1992. Response of regional seismicity to the static stress change produced by the Loma Prieta earthquake. Science 255, 1687-1690.

Saraò, A., Cocina, O., Privitera, E., Panza, G.F., 2010. The dynamics of the 2001 Etna eruption as seen by full moment tensor analysis. Geophys. J. Int. 181, 951–965. doi:10.1111/j.1365-246X.2010.04547.x.

Savage, J.C., Clark, M.M., 1982. Magmatic resurgence in the long valley caldera, California: possible cause of the 1980 Mammoth Lakes earthquakes. Science 217**,** 531–533.

Stein, R. S., 1999. The role of stress transfer in earthquake occurrence. Nature 402, 605–609.

Tarquini, S., Isola, I., Favalli, M., Mazzarini, F., Bisson, M., Pareschi, M.T., Boschi, E., 2007. TINITALY/01: a new Triangular Irregular Network of Italy. Annals of Geophysics 50, 3, 407- 425.

Thomas, A.L., 1993. Poly3D: A three-dimensional, polygonal element, displacement discontinuity boundary element computer program with applications to fractures, faults, and cavities in the Earth's crust. M. S. thesis, Stanford University, Stanford, California – U.S.A.

Tibaldi, A., Groppelli, G., 2002. Volcano-tectonic activity along structures of the unstable NE flank of Mount Etna (Italy) and their possible origin. J. Volcanol. Geotherm. Res. 115, 277– 302.

Toda, S., Stein, R.S., Sagiya, T., 2002. Evidence from the AD 2000 Izu Islands earthquake swarm that stressing rate governs seismicity. Nature 419**,** 58–61.

Walter, T.R., Acocella, V., Neri, M., Amelung F., 2005. Feedback processes between magmatic events and flank movement at Mount Etna (Italy) during the 2002–2003 eruption. J. Geophys. Res. 110. doi:10.1029/2005JB003688.

Figure captions

Figure 1. Structural sketch map of Mount Etna: Provenzana Fault (PR); Pernicana fault (PF); Santa Venerina fault (SVF); Timpe fault system STF; Moscarello fault (MF); Tremestieri–Trecastagni fault (TTF); San Leonardello Fault (SLF); Central Craters (CC); South Rift and North - East Rift are also indicated. In the upper inset, the location of Mount Etna in the central Mediterranean area and a simplified geological map of eastern Sicily are also reported. The INGV-G-DEM is in the WGS84 reference system and the projection is UTM33.

Figure 2. a) Top view and b) prospective view of the boundary Element model built in Poly3D environment show spatial relationships between topography, faults, magmatic reservoir, eruptive fractures, sliding plane and faults. For structure legend see tables 1 and 2.

Figure 3. Sketch of four models proposed showing: M1) Inflation of Magmatic Reservoir (MR); M2A) Opening of South Dike (SD); M2B) Opening of North-East Dike (NED); M3) Transtensive movement of Sliding Plane (SP); the acting sources (red) and the receiver structures (black) are drawn. For faults legend see table 2.

Figure 4. Three dimensional view showing the pattern of ΔCFS produced by inflation of MR (M1) along modeled fault planes; Opening of SD (M2A); Opening of NED (M2B) and Transtensive movement of SP (M3). The color bar specifies the maximum and minimum ΔCFS values that are reported for each single structure in Tables 3-6.

Figure 5. Three dimensional view showing the pattern of the displacement produced by inflation of MR (M1) along modeled fault planes; Opening of SD (M2A); Opening of NED (M2B) and

Transtensive movement of SP (M3). The color bar specifies the maximum and minimum displacement values that are reported for each single structure in Tables 3-6.

Table titles

Table 1. Description of deformation source inputs used in the numerical modeling. Xc, Yc and Zc represent the location of the center, while L and W correspond to length and width for each source.

Table 2. Position and geometrical parameters of receiver fault planes modeled in Poly3D program (for symbols explanation see table 1).

Table 3. Coulomb stress changes and displacements (U) induced on considered structures (see table 1 and 2 for structure names) by the inflation of MR (model M1).

Table 4. Coulomb stress changes and displacements (U) induced on considered structures (see table 1 and 2 for structure names) by the opening of SD (model M2A).

Table 5. Coulomb stress changes and displacements (U) induced on considered structures (see table 1 and 2 for structure names) by the opening of NED (model M2B).

Table 6. Coulomb stress changes and displacements (U) induced on considered structures (see table 1 and 2 for structure names) by the transtensive movement of SP (model M3).

Triggering mechanisms of static stress on Mount~~t.~~ Etna volcano. An application of the boundary element method.

E. Privitera[1], A. Bonanno[2], S. Gresta[~~1,~~3], G. Nunnari[2], G. Puglisi[1]*

1) Istituto Nazionale di Geofisica e Vulcanologia, Osservatorio Etneo, Piazza Roma 2, I-95123 Catania, Italy.
2) Università degli Studi di Catania, Dipartimento di Ingegneria Elettrica, Elettronica ed Informatica.~~Dipartimento di Elettrica, Elettronica e dei Sistemi~~, Viale Andrea Doria 6, I-95125, Catania, Italy.
3) Università degli Studi di Catania, Dipartimento di Scienze Biologiche, Geologiche e Ambientali~~Dipartimento di Geologia e Geofisica~~, Corso Italia 57, I-95129 Catania, Italy,

Formatted: Line spacing: Double

Running Title: Coulomb stress changes at ~~Mt.~~Mount Etna

* Corresponding author:
Eugenio Privitera
Istituto Nazionale di Geofisica e Vulcanologia – Osservatorio Etneo
Piazza Roma 2, I-95123 Catania (Italy)
E-mail: eugenio.privitera@ct.ingv.it

Field Code Changed

Tel.: ++39 095 716 5844 – Fax ++39 095 716 5826

Abstract

In the last thirty years, numerous eruptions and associated deformation episodes have occurred at Mt. Etna volcano. Datasets recorded by continuous Continuous and intense dynamics monitoring of these episodes magmatic processes provide a unique opportunity possibility to study the relationships between volcanism, flank instability and faulting activity. We have investigated the stress triggering mechanism between magmatic reservoir inflation, intrusive episodes and flank dynamics. Using three-dimensional numerical Boundary Elements Models we simulated volcano-tectonic events and calculated Coulomb stress changes. Using this Our modeling approach, we analyzed four realistic scenarios that are representative of represent recent kinematics episodes occurring at Mt. Etna well. The main results obtained highlight how (1) the inflating inflation of a deep spherical magma source transfers elastic stress to a sliding plane and faults (2) the opening of the NE Rift and S Rift (to a less efficient extent) favor movements of the instable sector and may encourage seismicity on the eastern flank faults, and (3) the flank instability may trigger the uprising of magma.

Defining the effects of the elastic stress transfer and relationships among the main forces acting on volcano, may help to forecast the possible eruption scenarios during future eruptive episodes of unrest at Mount Etna, – and provide an important tool for decision makers during volcanic emergencies involving the highly populated areaswhich is important to reduce volcanic and seismic hazards on the highly populated eastern sector of the volcano.

Keywords: Numerical modeling, Coulomb stress changes, flank instability, volcano dynamics, Mt.Mount Etna volcano, magmatic activity.

1. Introduction

Active volcanoes in densely populated areas represent a primary hazard that requires a operative and well-timed interaction between research institutions and civil defence authorities during unrest episodes. Consequently, involved researcher are encouraged to tune up affordable methods that can provide realistic scenarios of the eruptive evolution in near real-time.

Mount Etna dynamics is the result of a complex interplay between magma ascent in the plumbing system, dike emplacement, tectonic uplift, faulting and flank instability. ~~At Mount Etna, m~~Many studies have ~~evidenced~~highlighted that at Mount Etna increases in static stress induced by dike intrusions bring faults closer to failure (Gresta et al., 2005). More recently, the pressurization of a magmatic reservoir was considered to trigger 1997-1998 Mount Etna seismic swarms as ~~effects~~a consequence of stress redistribution (Bonanno et al, 2011).

The increase in collected seismic and deformation measurements and the rapid growth of computational power have enabled improving investigations into the relationship between faulting, flank dynamics and magmatic activity using numerical modeling. Walter et al. (2005) modeled the 2002-2003 Mt. Etna eruption by means of Boundary Element Method, evaluating the influence of four different sources on the kinematics of the volcano's eastern flank. They found a feedback relationship between flank movements and intrusive processes The numerical models suggest that magmatic activity (inflation of a reservoir and emplacement of dikes) encourages motion of the eastern flank, which, in turn, promotes magma to rise up to shallower levels within the volcano. Currenti et al. (2008) performed a Finite Element Modeling approach to evaluate ground deformation and the resulting stress redistributions in response to magmatic processes occurring during the 2002–2003 Etna eruption. They found that the changes in the state of stress generated by the southern dike produce an extensional stress field that favors magma propagation along the north-east Rift. The static stress changes computed onto the Timpe Fault System and the Pernicana

Fault indicate that the magma intrusions on the southern and northeastern flanks prompted these seismogenic structures to slip.Volcano flank instability has been recognized at many volcanoes around the globe. Dynamics of a flank is driven by combinations of gravity, magma pressure, lack of buttressing support, presence of an underlying weak substrate to the edifice, increasing pore pressure associated with volcanism, dyke emplacement, tectonic uplift and faulting (e.g. Siebert, 1984; McGuire, 1996; Merle and Borgia, 1996; Voight and Elsworth, 1997; Tibaldi, 2001; Acocella et al., 2006). In some cases, the interaction of several factors may make defining the main triggering cause of the instability difficult (Voight and Elsworth, 1992).

The increase in collected deformation measurements and the fast growth of computational power have permitted better investigating the relationship between flank dynamics and magmatic activity using numerical modeling. In this last decade, a significant proliferation of numerical modeling studies have highlighted that eruptions, flank instability and faulting episodes are related. Through limit equilibrium methods (LEM) and finite difference modeling (FEM), a 2D stability analysis of the NW flank of the Stromboli edifice was performed by Apuani and Corazzato (2009). The authors show that the tectonic seismicity of the area alone does not destabilize the studied slope. On the contrary, magma pressure in dykes can represent a destabilizing factor. Walter et al. (2005) modeled the 2002-2003 Mt. Etna eruption by means of Boundary Element Method, evaluating the influence of four different sources on the kinematics of the volcano’s eastern flank. They found a feedback relationship between flank movements and intrusive processes The numerical models suggest that magmatic activity (inflation of a reservoir and emplacement of dykes) encourages motion of the eastern flank, which, in turn, encourages the rise of magma to shallower levels within the volcano. Using Coulomb stress simulations, Segall et al., (2006) have demonstrated that a recent dike intrusion probably triggered a slow fault-slip event on Kilauea volcano's mobile south flank.

At Mount Etna, many studies have evidenced that increases in static stress induced by dike intrusions bring faults closer to failure (Gresta et al., 2005). More recently, the pressurization of a

~~magmatic reservoir was considered to trigger seismic swarms as effects of stress redistribution (Bonanno et al, 2011).~~

In this paper, we will use numerical simulations to hypothesize four realistic scenarios at Mt Etna in which one source at a time is active. Coulomb stress changes will be computed on three dimensional fault surfaces in order to investigate the interaction between intrusion/eruptive episodes, tectonic activity and flank instability. ~~. Understanding which factor influences the instability of the Mt. Etna volcanic edifice is therefore crucial for hazard assessment and mitigation.~~ The method used requires a processing time of some tens of minutes and is thus suitable for a near real-time application in order to forecast the evolution of future unrest episodes.

2. Etna volcano setting

Mount~~t.~~ Etna is a Quaternary basaltic stratovolcano located on the east coast of Sicily. It stands between two first-order tectonic elements: the Apenninic-Maghrebian Chain and the Hyblean Foreland (inset of Figure 1). The northern and western sectors of the volcano lie over metamorphic and sedimentary rocks belonging to the frontal nappes system of the Apenninic-Maghrebian Chain, whereas the southern and eastern sectors overlie marine clays of Quaternary age, deposited on the flexured margin of the northward-dipping downgoing Hyblean Foreland (Lentini, 1982) (inset of Figure 1).

Volcanic Activity

Recent volcanic activity of Mount Etna is characterized by eruptions at the four summit craters, and by fissure eruptions and dike intrusions at the rift zones oriented NE, south and west. During the last 400 years, about half of the eruptions occurred along the rift zones through fissures opened on the volcano flanks (Behncke and Neri, 2003). These fissures are usually related to the lateral intrusion of dikes radiating from a shallow magma conduit system.

Important results obtained during recent decades, mainly due to the rapid improvement in the seismic and deformation monitoring networks, have identified the main tectonic structures and the paths along which the magma rises beneath Mount Etna. Seismic tomographic images define the basement of Mount Etna as characterized by a main upper and middle crustal intrusion complex, with high V_p values (High Velocity Body; HVB), whose top is located at about 4 km below sea level (b.s.l), beneath the southeastern flank of Mount Etna (e.g., ~~i.e.~~ Aloisi et al., 2002; Chiarabba et al., 2004; Patanè et al., 2006). In recent years, magma intrusions have ascended along the western boundary of the HVB, as documented by ground deformation and seismic studies (e.g., Bonforte et al., 2008; Puglisi et al., 2008 and references therein). It is noteworthy that the lack of evidence for large magmatic storage volumes strongly supports the idea that, during its ascent along the western boundary of the HVB, the magma is stored as a plexus of dikes or sills, as suggested by Armienti et al. (1989) to justify the typical polybaric evolution of the magmas within the plumbing system of Mount Etna (Corsaro and Pompilio, 2004).

Structural framework

The shallow geodynamic behavior of Mount Etna seems to be controlled by the flank instability processes ~~implying~~ causing the seaward sliding of the volcano eastern side as a result of a complex interaction between regional tectonic stresses, gravity forces acting on the volcanic edifice and the ~~dyke~~dike-induced rifting (Neri et al., 1991; Borgia et al., 1992; Lo Giudice and Rasà, 1992; McGuire,1996; Rasà et al., 1996).

Although the published models propose different explanations of the origin and depth of the flank movement, they all agree in identifying the Pernicana Fault system, PF (Figure 1) as the northern boundary of the unstable sector. This is a transtensive fault with left lateral movement. It is characterized by a high slip rate from 10 to 28 mm/year with shallow (<3.5 km) and moderate seismic activity ($2<M<4.5$) (Azzaro, ~~et al., ~~1997; Azzaro et al., 2001). The PF activity is kinematically connected to the episodic opening and eruptions of the nearby NE Rift (Figure 1) (Neri et al., 1991; Gardunõ et al., 1997; Tibaldi and Groppelli, 2002; Acocella and Neri, 2003; Acocella et al., 2003). The southern part of the western boundary of the unstable sector is represented by the South Rift (Rasà et al., 1996) joining, southeastward, with the Tremestieri-Trecastagni fault system TTF (Figure 1). This fault system is made up of a number of NNW-SSE striking faults showing evident right-lateral displacement and is also characterized by very shallow seismicity, with typical focal depths of 1–2 km. Other tectonic lineaments dissect the southern and south-eastern sectors of the volcano, such as the Timpe Fault system (STF1 and STF2), San Leonardello Fault (SLF), Moscarello Fault (MF) and Santa Venerina Fault (SVF) (Figure 1).

Most of these faults have high slip~~-~~rates from 1.0 to 2.7 mm/year (Azzaro, 2004; Puglisi et al., 2008), partly due to shallow seismicity (Lo Giudice and Rasa, 1992; Montalto et al., 1996). Instrumental data, according to historical and macroseismic information (Azzaro~~ et al.~~, 1999), indicate that more than 80% of earthquakes are shallower than 5 km (Gresta et al., 1990), which~~where~~, despite their moderate magnitude, have often produced coseismic surface faulting. Fault plane solutions of these events frequently indicate a right lateral strike, combined with ~~an importanta~~a significant normal component.

More recent proposals emphasize the complexity of the unstable sector, showing how these faults represent the main structures that separate portions with slightly different velocities of downslope movement ~~of this sector of the volcano~~ (Bonforte et al., 2011).

3. CFS Modeling

In this paper, we investigate the relationships between volcanism, flank instability and ~~the~~ faulting ~~activity~~ in terms of elastic stress change. We investigate ~~hypothesize the~~ possible triggering conditions in which only one deformation source at a time is active. Our modeling approach

~~investigates~~ examines how (1) the inflation of a spherical deep source interacts with the sliding plane and faults, (2) the opening of an eruptive fissure (at North-East or South Rift zone) affects the sliding movement of eastern sector or seismic activity on fault planes, (3) the flank instability governs the kinematics of faults and triggers (or inhibits) the ascent of magma (Figure 3).

3.1. Modeling Method

Taking into account the topographic effects, we compute boundary element solutions of deformation sources e~~i~~mbedded in an elastic half-space, using the program Poly3D 2.1.8 (Thomas, 1993; Maerten et al., 2005). Based upon the boundary element method~~, BEM~~ (Crouch and Starfield, 1983), Poly3D includes the fundamental solution to an angular dislocation in a homogeneous, linear elastic half-space (Comninou and Dundurs, 1975). A number of angular dislocations are juxtaposed to create polygonal boundary elements that collectively define discretized objects of arbitrary shape in three dimensions. Boundary conditions in Poly3D can be applied remotely (as constant stresses or strains), at the centers of each element of the discretized fault surface (as tractions or displacement), or as combinations. The program solves a series of linear algebraic equations that describe the influence of ~~on~~ each element ~~of~~ on every other element under a prescribed set of boundary conditions. Once the displacement distribution along a fault is determined, the static stress, strain and displacement fields around the fault are calculated using influence coefficient equations that relate the displacements at the fault to the resultant elastic field at any point in the surrounding linear elastic medium. This solution is superimposed upon the remote stress field boundary condition to produce the total elastic field. Note that in our modeling processes we do not take into account the regional stress field. Indeed, geological and geophysical evidences highlight the heterogeneity of the Mount Etna stress field in time and space (e.g., Barberi et al., 2000 and reference therein). According to Gresta et al. (2005), from a kinematic point of view, the coexistence of structural elements such as PF and TFS are incompatible with a homogeneous stress field. Consequently, in this paper we use only “Specified fault calculation” for ΔCFS computation and we relinquish the evaluation of ''optimally oriented faults'' (strongly influenced by the regional stress field) as suggested by several authors in such cases (e.g., Gresta et al. 2005, Bonanno et al., 2011 and references therein)

In Poly3D we build polygonal elements for modeling complex surfaces with curving boundaries. Surface fault changes in strike are meshed without gaps. The spherical void is built by assembling triangular, hexagonal or pentagonal elements in the same manner as a football.

The Boundary Element Method was chosen because it is suitable for near real-time applications since it allows modifying an evolving scenario simply by adding new magmatic sources and/or receiving structures. The use of Poly3D enables avoiding meshing the medium every time a structural modification is carried out, in such a way the computational time is limited to tens of minutes.

3.2. Setup of deformation source parameters

Following on from In agreement with recent geophysical evidencesstudies (Patanè et al., 2003a; Chiarabba et al., 2004; Bonaccorso et al., 2006; Bonforte et al., 2008; Puglisi et al., 2008; Chiarabba et al., 2004; Patanè et al., 2003b), we considered a spherical cavity constructed by of 815 triangular elements, simulating a 1 km in radius reservoir 1 km in radius at 3 km depth (Figure 2). An increase in the magma pressure perturbs the stress field in the surrounding crust. Using positive traction boundary conditions, normal to the element, we defined a volume increase of $7.9*10^6$ m^3, a realistic value for inflating magma bodies (Bonaccorso et al., 2006; Palano et al., 2007; Puglisi et al., 2008). The center of the MR was located beneath the Summit Craters area (for details see Table 1). In addition, in order to evaluate the influence of the depth of an inflating reservoir (hereafter MR) on the other considered structures and in particular on SP, , we performed two further simulations moving the center of the sphere by ± 2.4 km. These steps of depth were chosen since they roughly correspond to the projections respectively of the top and the bottom of SP (see below) along the vertical line intersecting the Summit Craters.

~~The center of the MR was located beneath the Summit Craters (for details see Table 1).~~ ~~Dyke~~Dike intrusions were modeled by rectangular planes with a curving top boundary matching the topography (Figure 2). A uniform element-normal displacement discontinuity of 2.5 ~~meters~~m is imposed on ~~dykes~~dikes. The geometry of the North-East and South dikes used in this paper is based on values published by Puglisi et al. (2008). In any case, openings larger than 3 m do not modify the results significantly. The parameters of the modeled dikes are reported in Table 1.

In agreement with ~~to~~ inversion models inferred from ground deformation measurements (Puglisi and Bonforte, 2004; Bonaccorso et al., 2006; Bonforte et al., 2008), we modeled a sub-horizontal sliding plane (hereafter SP) as a rectangular surface ~~long~~ 20 km long and ~~wide~~ 25 km wide, with a main normal (7.7 cm) and minor dextral component (4.4 cm) (Figure 2). Although the slip amount depends on the period investigated, inversion models published (Puglisi and Bonforte, 2004; Palano et al, 2007) found an overall sliding in the range of 4 – 9 cm/year in the period 1993 -2000.

3.3. Setup of topography and fault parameters

We used the Global Digital Elevation Model (~~hereafter the~~ INGV-G-DEM) that merges inland DEM (Tarquini et al., 2007; Neri et al., 2008) and bathymetric data sets available for the ~~Mt.~~Mount Etna area (Bosman et al., 2007; Cavallaro et al., 2008). The original data ~~are~~ were integrated and interpolated, becoming homogenous with a final resolution of 10 m pixel size. Using INGV-G-DEM resampled with a resolution of 100 m, we buil~~d~~t a rectangular surface of 3500 km^2 (extending for about 70 kilometers in longitude and 50 km in latitude) and discretized with 3184 triangular meshes (Figure 2). Volcano topography is assumed as a traction-free surface in order to study the influence on displacements and stress numerical calculations. According to geological and structural studies integrated with seismic data, we modeled the main tectonic lineaments of the eastern sector of the volcano. We buil~~d~~t the faulting planes as rectangular surfaces with a curving top boundary matching the topography, with each plane ~~is~~ discretized by triangular meshes with a mean areal dimension of about 0.027 km^2. In particular, Provenzana Fault (PR) shows a change of strike from N35°E to N55°E, thus a curving top boundary is modeled. The Pernicana Fault (PF) is ~~composed~~ made up of four segments~~,~~ ~~defined~~ (PF1, PF2, PF3 and PF4)~~,~~ striking N88°E, N102°E, N114°E, N120°E, respectively (Figure 2a). The southern border of the unstable sector is represented by the Tremestieri-Trecastagni Fault system (TTF) modeled with a sub-vertical plane with a sharp change in direction (from N103°E to N150°E). The Timpe Fault System is made up ~~to~~ of two segments, STF1 and STF~~-~~2, with strike direction N165°E and N3°W, respectively. These latter fault systems, together with SLF, MF, SVF, all striking from N173°E to N140°E, reach~~ed~~ the depth of the sliding plane (see Figure 2b). The sub-vertical fault~~s~~ planes above the sliding plane (SP) have a width ranging from 1950 to 2800 ~~meters~~m (for details see Table 2). In our models, we assume that receiver faults are discontinuities embedded in an elastic half-space in which they are free to move in any direction.

3.4 Coulomb Stress Changes

We calculated Coulomb stress changes caused by volcanic sources on modeled fault planes, while computing changes in volumetric or normal stress near the magma chamber or eruptive dikes caused by flank movements or earthquakes (e.g. Savage and Clark 1982; Nostro *et al.* 1998; Toda *et al.* 2002).

Formatted: Line spacing: Double

It is widely accepted that static stress changes (≥ 0.1 bars) induced by a magmatic source may trigger seismicity within a rock volume close to the critical state of failure (e.g., Reasenberg and Simpson, 1992; Stein, 1999). Spatial and temporal relationships between stress changes and earthquakes are explained through the Coulomb failure stress change, defined as:

$$\Delta CFS = \Delta\tau + \mu(\Delta\sigma_n + \Delta P) \qquad (1)$$

where $\Delta\tau$ is the shear stress change computed in the direction of slip on the fault, $\Delta\sigma_n$ is the normal stress change (positive for extension), μ is the coefficient of friction and ΔP is the pore pressure change (e.g., King *et al.*, 1994; Harris, 1998; King and Cocco, 2000). For simplicity, we considered here a constant effective friction model (Beeler *et al.*, 2000; Cocco and Rice 2002) that ~~, which~~ assumes ~~that~~ ΔP is proportional to the normal stress changes ($\Delta P = -B\Delta\sigma_n$, where B is the Skempton parameter):

$$\Delta CFS = \Delta\tau + \mu'\Delta\sigma_n \qquad (2)$$

where μ' is the effective friction ($\mu' = \mu[1 - B)]$). The fault is brought closer to failure when ΔCFS is positive. In order to verify if dike intrusions or magmatic reservoir inflations are encouraged, we evaluate the change of the volumetric strain ($\Delta\varepsilon = \varepsilon_1 + \varepsilon_2 + \varepsilon_3$) on the magmatic reservoir and horizontal normal stress changes ($\sigma_m = \Delta\sigma_{xx} + \Delta\sigma_{yy}) / 2$) on the rift zone dikes. Indeed, the unclamping of a rift zone ($\sigma_m>0$) induced by fault dislocations may facilitate the ascent of new magma and dike injection. In the same way, the unclamping may favor the decompression of the magma reservoir, leading to the formation and ascent of bubbles and then increasing the magma overpressure. We performed all calculations in a homogeneous Poissonian elastic half-space using a Poisson~~'s~~ ration of $\nu = 0.25$ and a Young~~'s~~ modulus of E = 75 GPa, and a $\mu' = 0.4$.

3.5 Assumptions of numerical modeling

Coulomb stress changes are evaluated in a homogenous elastic half-space. Thus mechanical heterogeneities, for instance due to thermal structure, a hydrothermal altered volcanic core or a mechanically rigid basement, are not taken into account by our models. As stated before, the regional stress field is not taken into account given its heterogeneity in space and time. The surface traces of the faults are visible, well-mapped and constrained, but we simplif~~y~~ied the characteristics of the sliding plane by imposing a uniform slip on the whole rectangular surface. We ~~do~~ did not take into account visco-elastic or elasto-plastic behaviors or any differential flank movement ~~supposed~~ inferred by a number of authors recently (Palano et al., 2009; Currenti et. al, 2010;Bonforte et al., 2011~~; Palano et al., 2009~~).

4. Modeling

For each model, ΔCFS values are computed on faulting planes and on the sliding surface (Figure 2). The normal stress σ_m is evaluated on dike fractures and volumetric strain Δε on the spherical surface of magmatic reservoir. The parameters of sources and receiver structures are described in Table 1 and 2, respectively. Four deformation models were tested:~~have been carried out:~~ M1, inflating of a spherical magmatic source (Figure 3, M1); M2, opening of eruptive fissures (Figure 3, M2), divided into two models A) for South dike and B) North East dike; and M3, sliding of planar surface (Figure 3, M3). Our numerical results of ΔCFS on each receiver structures are ~~summarized~~ reported in Tables 3-6.

4.1. Model 1 - Mogi Source

a) Stress calculations

We first considered stress changes associated with a reservoir inflation (depth = 3.0 km, roughly coincident with the center of the SP). ~~The~~ M1 shows a decrease of CFS along the PR and PF2 segments~~.~~ and an increase along the PF1 segment, ~~has experienced positive stress~~ with the latter showing a ~~a~~ maximum value of 1.4 bars along the western edge (see M1 in Figure 4~~, M1~~and Table 3 for maximum and minimum ΔCFS values). A decrease and an increase close to zero ~~are~~ were computed on PF3 and PF4 planes, respectively (Table 3). ~~The inflation of magmatic reservoir~~M1 induces ~~on STF1 and on SVF~~ a stress increment on STF1 and SVF ~~on the~~ closer portions (0.3 and 0.2 bars). The MF, SLF and TTF planes are subjected to a slight positive increment on the top edge (in a range between 0.1 and 0.2 bars) (Figure 4, M1). Moreover, the movement of STF2 is inhibited by the inflation of MR. Finally, the inflation of spherical chamber favors the closure of the NE and South dikes significantly. On the sliding plane, we observed a decrease of ΔCFS in the northwestern part of the plane (minimum value about -2 bars) and a very slight positive variation (0.2 bars) along the remaining part of the surface.

The simulations performed moving the depth of MR do not change the scenario described before drastically and significant variations only affect a few structures. A shallow MR (depth = 0.6 km; roughly coincident with the top boundary of the SP) does not change the pattern of the static stress on all the faults considered, and the intensity is only slightly affected. Also the NE dike shows almost unaltered features and only a very small part of the dike (near MR) underwent an unclamping effect. The most important variation is observed on the SP, which experienced a positive CFS variation ~~until~~ of 2 bars. ~~Also~~ The S dike also showed a different pattern in ΔCFS distribution; indeed, the closure of the S dike is strongly encouraged only in the portion near MR, while the remaining part underwent an unclamping effect. The inflation of a deeper MR (depth = 5.4 km; roughly coincident with bottom boundary of the SP) does not change the static stress pattern on the SP and the S and NE ~~dykes~~dikes. A slight change in the intensity affected both dikes, enhancing the closure trend observed with a 3 km depth MR. Also the majority of the faults considered show unchanged features and only MF experienced a positive CFS variation until 1.4 bars.

In summary, the depth of an inflating shallow crustal reservoir may change the scenario evaluated slightly and only the flank movement seems significantly affected by the depth of MR; indeed, very shallow MR may promote flank movements, while deeper MR inhibits them. In general, a shallow ~~crust~~ MR discourages dike intrusion into the Mount Etna rift zones and promotes the stress triggering on the westernmost portion of PF.

b) Displacement calculations

The expansion of MR a~~the magmatic reservoir a~~t 3 km depth induced the uplift of the nearby structures, such as PR, PF1 and PF2 (see Figure 5 and Table 3 for maximum and minimum displacement values). The inverse component is replaced by left~~-~~lateral movement on PF3 and PF4 components. The displacement values are progressively reduced from the western to eastern part. SLF, STF2, TTF and MF shows a right-lateral movement. On STF1, SVF and SP planes an uplift is favored. In particular, on the ~~Sliding Plane (~~SP~~)~~ a maximum value of 2.4 centimeters ~~as~~ of thrust movement is computed. This result changes drastically if we consider a very shallow crustal reservoir, which ~~that~~ inverts the observed trend, promoting seaward movements of the eastern flank. It is clear that for this aspect of the problem the boundary condition set in the model (source depth) plays a basic role and highlights just how crucial the depth constraint is in ground deformation inversion analyses.

4.2. Model 2A – South Dike

a) Stress calculations

Intrusion along the ~~of~~ S dike favors the closure of NE dike with a negative unclamping effect (σ_m maximum value is about of -32 bars). In the M2a we observe ~~PR segment with~~ a decrease of ΔCFS on the PR segment (max value -4.5 bars). On the PF system ΔCFS values are negative except on PF1 with a positive stress variation reaching a maximum value of 1.4 bar on the upper part of plane (Table 4). PF2, PF3, PF4 and SLF segments show a slight increase but in general all planes show ~~are involved with~~ a reduction of ~~stress changes~~ ΔCFS. STF1, STF2, SVF and TTF similarly underwent a reduction of ΔCFS ~~stress effect~~ (see M2A in Figure 4 and Table 4 for maximum and minimum ΔCFS values~~, M2A).~~). On SP a maximum positive stress change is computed for ~~evaluated on~~ the part of the plane ~~closer~~ closest to the magmatic feeding system. Finally, the S-dike ~~south~~ intrusion induces a compression (ε>0) on the MR ~~magmatic reservoir~~ located beneath the summit craters (see Figure 4, M2A).

b) Displacement calculations

The opening of SD encourages a normal movement of SP. The direction of displacement vectors on SVF, SLF, STF1, STF2 and MF shows a right~~-~~-lateral movement associated with the ~~to~~ dip~~-~~-normal component. PR and TTF segments show the reverse ~~underwent an inverse~~ movement. All PF segments move with a pure left~~-~~-lateral strike slip (see Figure 5 and Table 4 ~~4~~ for maximum and minimum displacement values~~for details on the amount of slip~~). In summary, magmatic activity in the South Rift closes~~?~~ the North East Rift and mobilizes the East and North East region of the unstable block.

4.3. Model 2B – North East Dike

a) Stress change calculations

In M2B we find that intrusion along the ~~of~~ NE dike into the rift zones causes significant increase of ΔCFS on PR and PF1, with maximum values of about 320 bars and 100 bars, respectively. On the upper part of PF2 ~~fault~~ elastic stress changes increase to 3.4 bars. PF3, STF1, SVF, STF2 and TTF show a decrease of static stress variations (Table 5). SLF and MF are brought close to failure on the shallower portions of fault planes with higher values of 2.3 and 5.3 bars, respectively (see M2B in Figure 4 and Table 5 for maximum and minimum ΔCFS values~~, M2B~~). A significant negative unclamping effect on the walls of the S dike is found (max σ_m value about of -26 bars). The opening of the NE dike favors the decompression of ~~magmatic reservoir~~MR with ε_{max} about of -4.8e-5 m^3(ε<0 volumetric strain is negative for decompression). Finally, we observe that because of its dimension and geometry, the NE dike is more efficient in ~~shows stress~~ transferring stress ~~mechanism~~ on the sliding plane ~~more efficiently~~ with respect to the S dike. On the shallower portion of SP the maximum value of ΔCFS reaches 2.6 bars (Table 5).

b) Displacement calculations

The most important results regarding displacement calculations show that the opening of the NE dike favors the sliding of flank with a transtensive component (see Figure 5 and Table 5 for maximum and minimum displacement values). All modeled faults, such as TTF, SVF, STF1, STF2, MF and STF are kinematically compatible with a right-lateral movement associated to with a normal dip component. On PR, PF1 and PF2 planes a transpressive left--lateral movement is favored. Towards the eEast we found only left transcurrent component on PF3 and PF4 structures.

4.4. Model 3 – Sliding Plane

a) Stress calculations

We find found a positive ΔCFS with max values of about 1.7 and 1.5 bars in the upper part of PF1 and PF2, respectively, and. On the contrary, we evaluated an increase of static stress in the lower portion of PF3 and PF4 (max about of 3.5 bars). The relative position between SP and receiver faults also resulted in an increase in conditioned the increasing of static stress on TTF plane also. Thus, we estimated a positive ΔCFS in the lower part of this structure with a maximum value of 3 bars (see M3 Table 6 andin Figure 4 and Table 6 for maximum and minimum ΔCFS values, M3). Small increases of elastic stress are evaluated found on the MF, SLF, SVF, STF1 and SFT2 faults (Table 6). The sliding of the plane beneath the eastern flank seems to favor a compression for a magmatic reservoir (MR) (ε>0 volumetric strain is positive). The unclamping effects for two vertical eruptive fractures located on the northeast and southern flank of volcano is was estimated. We find observed that SP induces the closure in the upper part of tabular dikes. Instead, a small opening is favored in their deeper zones (about 0.1 bars) (Figure 4, M3). This interaction depends on the dimension of modeled eruptive fractures and the depth of sliding planeSP. In brief, the unstable condition of flank sliding toward the sea may affect the magmatic system. Decompression of plumbing system may lead to the ascent of new magma or modify the condition of overpressure with the formation of bubbles (Hill, 2002).

b) Displacement calculations

The results of our simulations (see Figure 5 and Table 6 for maximum and minimum displacement values) show that the transtensive movement of SP encourages the dip normal displacement on PR, PF1 and PF2. By contrast, ~~On contrary,~~ PF3 and PF4 moves according to a dip-~~-~~normal associated to a left lateral movement. Coherently to observed kinematics STF1, STF2, SLF, SVF and MF are encouraged to move with a transtensive component, whereas a ~~. Instead,~~ transpressive movement is determined ~~evaluated~~ for TTF.

5. Discussion and conclusions

During these last decades ~~Mt.~~Mount Etna volcano has ~~experienced~~ undergone several eruptions that have highlighted ~~of different nature highlighting~~ intriguing trigger mechanisms and have featured ~~among~~ dike intrusions, activation of seismogenic faults and aseismic ground deformations. ~~For instance, in 1985 and 1986 (Azzaro, 1997) the simultaneous occurrence of significant earthquakes on Provenzana - Pernicana fault systems and the opening of the eruptive fracture some kilometers away occurred, but the lack of good quality ground deformation data hindered the understanding of the causal relationship.~~

~~The different patterns of ground deformation observed on Mt. Etna volcano during the last decade through GPS and InSAR data have enabled modeling the complex volcano-tectonic phenomena that have occurred. In detail, both point sources (Mogi) and planar dislocations (i.e. Bonforte et al., 2008; 2011; Palano et al., 2008) have been widely used. Point pressure sources roughly take into account the radial component of the deformations occurred with respect to the central plumbing system, whereas planar sources well-represent the deformation field produced by the dikes opening (tensile sources) and by faults or the seaward sliding of the eastern sector of the volcano, respectively (strike-slip or dip-slip sources).~~

~~On the whole, irrespective of the numerical results (i.e. source depth and/or dimensions), point pressure sources and planar dislocations have fully satisfied the need for modelling the different ground deformation patterns observed during the different states of the volcano dynamics. In some cases (i.e. Palano et al., 2008), the simultaneous effect of at least two different sources was invoked to better fit the measured deformations.~~ Geophysical studies suggest that complex dynamics, involving more than one source (seismogenic sources and ~~dykes~~dikes), is a relatively common characteristic of eruptive episodes on ~~Mt.~~Mount Etna. Gresta et al. (2005), for instance, ~~had~~ highlighted that earthquakes along the PF and STF were induced by the static stress variations associated ~~to~~ with the emplacement of eruptive dikes during the 1981 and 2001 eruptions, respectively. More recently, the pressure increase due to magma ascent episodes occurring in 1997-1998 at ~~Mt.~~Mount Etna has been demonstrated to be responsible for the reactivation of seismogenic structures on the western side of the volcano (Bonanno et al., 2011). In Bonanno et al. (2011), the intrusive process was modelled as an inflating Mogi source located at 5.5 km depth, but in the present work, we ~~highlight~~ emphasize the crucial role of the boundary condition set in the model (source depth) and ~~we~~ show the possible scenarios with a shallower MR depth (Model M1).

~~Gresta et al. (2005) highlighted that earthquakes along PF and STF were induced by the static stress variations associated to the emplacement of eruptive dikes during 1981 and 2001 eruptions, respectively. In greater detail, t~~The July-August 2001 eruption was characterized by a very complex field of flank eruptive fractures located largely on the upper southern slope of the volcano (Monaco et al., 2005). The eruption onset was preceded and accompanied by significant earthquakes (Patanè et al., 2003b) and marked ground deformations (Bonaccorso et al., 2002). The main source of deformations was modelled by a tensile dislocation located on the South Rift zone (Puglisi et al. 2008) as also confirmed by the Seismic Moment Tensor inversions of the best constrained earthquakes that heralded the opening of the eruptive fractures (Saraò et al., 2010). Our present model M2A takes ~~into~~ account of the main behaviour of the magmatic source for this eruption well.

The October 2002 - January 2003 eruption occurred on two sides of the volcano, along the upper north-eastern (NE Rift zone) and southern (South Rift Zone) flanks. Once again, earthquakes and ground deformations preceded and accompanied the opening of the eruptive fractures ~~notably~~ (Barberi et al., 2004 and reference there in). The two intrusive dikes have been satisfactorily modelled by two separate tensile dislocations (Aloisi et al., 2003). During the first stage of the eruption, several seismogenic structures on the eastern flank became successively active. This was explained as due to the transfer of elastic stress from the magmatic source to faults (PR and PF) and afterwards from faults to faults (Barberi et al., 2004). Our present model M2B is schematically representative of the first stage of the above cited domino effect phenomena.

Finally, the 2004–2005 eruption emitted a highly degassed magma from a sub-terminal fracture. During the first weeks of activity, the erupted magma was already residing inside the volcano, probably since the 2002-2003 eruption, while later it mixed with new magma ~~a new one~~ ascending through the central conduit~~s~~ system (Corsaro et al., 2009). Magma intruded passively due to the exceptional extension on the summit area caused by the large sliding of the eastern flank of the volcano (almost 9 cm of slip; Bonaccorso et al., 2006). The east flank sliding toward the sea ~~is able to~~ induces a decompression on the shallow magma plumbing system as foreseen by our model M3 that simulates the unstable condition of this sector.

In this work we have investigated, by using the Boundary Element Method, how (*i*) the inflating of a deep spherical source interacts with a sliding plane and with faults and rift elements; (*ii*) the opening of eruptive fissures affects the sliding movement of the eastern sector of Mount Etna, encouraging earthquakes ~~occurrence~~ on fault planes; and (*iii*) the instability of the eastern flank governs the kinematics of faults and/or triggers the ascent of magma.

Formatted: Line spacing: Double

The results presented here are strongly dependent on all the assumptions made. In particular, the lack of seismological constraints (hypocenter patterns and compatible fault plane solutions) ~~to~~ for the sliding plane induced us to simplify the geometry of a detachment volume that remains/lies at the base of the instable sector. Nevertheless, our numerical results show good agreement with deformation measurements that well- describe the eastern flank dynamics of Etna volcano (e.g., i.e. Bonforte et al., 2008; Puglisi et al., 2008). The strength of our approach consists in evaluating the distribution of the CFS pattern along the receiver fault planes using numerical simulations, taking into account the effects of topography and with a processing time of about tens of minutes.

The main results obtained are the following:

1. The inflation of a magma reservoir encourages the slip on the westernmost segment of the Pernicana fault (PF).
2. The depth of MR is crucial, very shallow depth MR promote seaward movement of the eastern flank, while deeper MR (3.0 - 5.5 km) inhibit the movement.
3. Dikes intruding either on the NE or/and South Rift Zones favor the sliding of the planar source in its upper part and along the westernmost of PF.
4. The intrusion (opening) of a South dike favors the closure of a NE dike, while at the same time the opening of NE tensile fracture inhibits the ascent of magma along the South zone.
5. The intrusion of a NE dike (for dimension and kinematics) favors the Eastern flank sliding, more than the opening of an S dike.
6. The opening of a NE dike encourages the decompression of the magma plumbing system (depth = 3.0 km), evaluated by a high negative value of volumetric strain.
7. The passive sliding of SP promotes an increase of CFS on the westernmost and the central segments of PF. Its easternmost segments are brought close to failure at their bases.
8. The unstable condition of flank sliding toward the sea may affect the magmatic system and decompression of plumbing system may lead to a new magma ascent.
9. The western part of Pernicana fault (PF1) experienced a positive CFS for all the scenarios hypothesized. The other segments underwent a positive stress variation only in M2B and M3. In particular, Model M2B highlights the governing role of the intrusion in the NE Rift on the dynamics of this structure and on the dynamics of the Provenzana fault too.

10. Other faults considered seem to be less sensitive to the stress variation induced by sources considered, with the exception of three structures. SLF and MF underwent a significant positive CFS variation in model M2B, and TTF experienced an increase in static stress in model M3.

~~The above listed~~These results schematically represent possible scenarios of the evolution of the kinematic "activity" of ~~Mt.~~Mount Etna volcano. The three basic elements~~:~~ (magma dynamics, earthquake occurrence and flank instability) interact with each other, alternating their active or passive role in a broader combination of domino effects.

Our results are in ~~a~~ general agreement with the findings of Walter et al. (2005), despite the significant differences in the structural setup and in the definition of geometrical characteristics of the single geological objects. The main difference regards the effect of interaction between magma reservoir and sliding plane; ~~as a matter of fact,~~ the latter was defined by Walter et al. (2005) with geometrical characteristics that are entirely different from those hypothesized in this paper. Currenti et al. (2008) use a very simplified structural setup taking into account only the two rift zones and the main fault systems in eastern flank. Regardless of differences, the result obtained are similar with the exception of the NE dike response to an intrusion in the South rift. Currenti et al. (2008) have also demonstrated that the introduction of an heterogeneous medium induces variation in the intensity of ΔCFS (as a function of modelled elastic parameters), but does not distort the geometrical pattern. The authors also show how the stress shape is affected by Mt. Etna topography. The main discrepancies are largely restricted to the volcano summit area because of the accentuated topography.

We note that the strength of our approach lies in the fact that we evaluate the distribution of the CFS pattern while taking into account the relevant effects of topography. In addition, we use a method that requires a processing time of some tens of minutes.

It allows modifying an evolving erupting scenario simply by adding or alterating magmatic sources and/or receiving structures without needing any further computational time that other numerical methods require (e.g., re-mesh of medium in Finite Element Method). The real-time seismic and geodetic networks currently operating on ~~Mt.~~Mount Etna are able to provide good enough data (both in number and quality) to satisfactorily (and rapidly) constrain the source(s) responsible for volcanic unrest. The application of the Boundary Element Method during volcanic unrest appears ~~to be~~ a promising tool ~~for~~ to provid~~inge~~ ~~in near real-time~~ some possible scenarios of ~~the~~ evol~~ution~~ving ~~of the~~ volcan~~o~~ic activity in near real-time in terms of ~~eastern~~ flank sliding and/or activation of either (both) seismogenic faults and/or magma bodies.

Acknowledgments

This work was funded by the INGV-DPC project V4_Flank. We thank Stephen Conway for correcting and improving the English. Amalia Bonanno was supported by INGV-DPC fellowships.

We thank the editor Joan Marti and two anonymous reviewers for the careful revision that enabled improving the paper significantly. The DEM used in this paper is the result of the integration of data available at INGV, in particular the DEM_ Sicilia 1999 (Tarquini et al., 2007) and the DEM_Lidar 2005 (Neri et al., 2008). This DEM was produced in the framework of the ASI-SRV project, and INGV-DPC V4-Flank project, thanks to Dr. F. Guglielmino (INGV, Osservatorio Etneo).

References

Formatted: Italian (Italy)

Acocella, V., Neri, M., 2003. What makes flank eruptions? The 2001 Mount Etna eruption and its possible triggering mechanisms. Bull. Volcanol. 65, 517–529.

Acocella, V., Behncke, B., Neri, M., D'Amico, S., 2003. Link between major flank slip and 2002-2003 eruption at Mount Etna (Italy). Geophys. Res. Lett. 30(24), 2286. doi:10.1029/2003GL018642.

~~Acocella, V., Neri, M., Scarlato, P., 2006. Understanding shallow magma emplacement at volcanoes: Orthogonal feeder dikes during the 2002 – 2003 Stromboli (Italy) eruption. Geophys. Res. Lett. 33, L17310. doi:10.1029/2006GL026862.~~

Aloisi, M., Cocina, O., Neri, G., Orecchio, B., Privitera, E., 2002. Seismic tomography of the crust underneath the Etna volcano, Sicily. Phys. Earth Planet. In. 134, 139–155.

Aloisi, M., Bonaccorso, A., Gambino, S., Mattia, M., Puglisi, G., 2003. Etna 2002 eruption imaged from continuous tilt and GPS data., Geophys. Res. Lett. 30(23), 2214. doi:10.1029/2003GL018896.

~~Apuani T., Corazzato, C., 2009. Numerical model of the Stromboli volcano (Italy) including the effect of magma pressure in the dyke system. Rock Mech. Rock Engng. 42, 53-72. doi: 10.1007/s00603-008-0163-1.~~

Armienti, P., Innocenti, F., Petrini, R., Pompilio, M., Villari, L., 1989. Petrology and Sr-Nd isotope geochemistry of recent lavas from Mt. Etna: Bearing on the volcano feeding system. J. Volcanol. Geotherm. Res. 39, 315– 327. doi:10.1016/0377-0273(89)90095-4.

Azzaro, R., 1997. Seismicity and active tectonics along the Pernicana fault, Mt. Etna (Italy). Acta Vulcanol. 9, 7-14.

Azzaro, R., 1999. Earthquake surface faulting at Mount Etna volcano (Sicily) and implications for active tectonics. *J. Geodynamics* 28, 193-213. doi:10.1016/S0264-3707(98)00037-4.

Azzaro, R., 2004. Seismicity and active tectonics in the Etna region: Constraints for a seismotectonic model. In: Bonaccorso, A, et al. (Eds.), Etna Volcano Laboratory. Geophys. Monogr. Ser., vol. 143, AGU, Washington, D. C., pp. 205–220.

Azzaro, R., Mattia, M., Puglisi, G., 2001: Fault creep and kinematics of the eastern segment of the Pernicana Fault (Mt. Etna, Italy) derived from geodetic observations and their tectonic significance. Tectonoph., 333, 3/4, 401-415.

Barberi, G., Cocina, O., Neri, G., Privitera, E., Spampinato, S., 2000. Volcanological inferences from seismic straintensor computations at Mt. Etna Volcano, Sicily. Bull. Volcanol. 62, 318– 330.

Barberi, G., Cocina, O., Maiolino, V., Musumeci, C., Privitera, E., 2004. Insight into Mt. Etna (Italy) kinematics during the 2002–2003 eruption as inferred from seismic stress and strain tensors. Gephys. Res. Lett. 31, L21614. doi:10.1029/2004GL020918.

Beeler, N.-M., Simpson, R.-W., Lockner, D.-A., Hickman, S.-H., 2000. Pore fluid pressure, apparent friction and Coulomb failure. J. Geophys. Res. 105, 25533– 25554.

Behncke, B., Neri, M., 2003. Cycles and trends in the recent eruptive behaviour of Mount Etna (Italy). Can. J. Earth Sci. 40, 1405 – 1411. doi:10.1139/E03-052.

Bonaccorso, A., Aloisi, M., Mattia, M., 2002. Dike emplacement forerunning the Etna July 2001 eruption modeled through continuous tilt and GPS data. Geophys. Res. Lett. 29 (2), 1–4. doi: 10.1029/2001GL014397.

Bonaccorso, A., Bonforte, A., Guglielmino, F., Palano, M., Puglisi, G., 2006. Composite ground deformation pattern forerunning the 2004– 2005 Mount Etna eruption. J. Geophys. Res. 111, B12207. doi:10.1029/ 2005JB004206.

Bonanno, A., Palano, M., Privitera, E., Gresta, S., Puglisi, G., 2011. Magma intrusion mechanisms and redistribution of seismogenic stress at Mt. Etna volcano (1997-1998). Terra Nova 23, 339-348. doi: 10.1111/j.1365-3121.2011.01019.x.

Bonforte, A., Bonaccorso, A., Guglielmino, F., Palano, M., Puglisi, G., 2008. Feeding system and magma storage beneath Mt. Etna as revealed by recent inflation/deflation cycles. J. Geophys. Res. 113, B05406. doi:10.1029/2007JB005334.

Bonforte, A., Guglielmino, F., Coltelli, M., Ferretti, A., Puglisi, G., 2011. Structural assessment of Mount Etna volcano from Permanent Scatterers analysis. Geochem. Geophys. Geosyst. 12, Q02002. doi:10.1029/2010GC003213.

Borgia, A., Ferrari, L., Pasquarè, G., 1992. Importance of gravitational spreading in the tectonic and volcanic evolution of Mount Etna. Nature 357, 231– 235. doi:10.1038/357231a0.

Bosman A., Cavallaro, D., Chiocci, F.L., Coltelli, M., 2007. New insights on the Etna offshore reveal unknown morphological features related to the volcano eastern flank dynamics. Geoitalia 2007- Sesto Forum Italiano di Scienze della Terra. Rimini, 12-14 settembre 2007. ~~Vol 2, 2007~~ ISSN 1972-1552 pp. 117.

Cavallaro D., Lodi, M., Bosman, A., Chiocci F., Coltelli, M., 2008. Evidenze di faglie attive nell'offshore etneo rilevate da analisi morfos strutturali. Riassunti del 84° Congresso Nazionale Società Geologica Italiana~~, Vol.~~ 3~~, Fascicolo~~ /3, pp. 204-205. (in Italian)~~Sassari 15-17 Settembre 2008.~~

Chiarabba, C., De Gori, P., Patanè, D., 2004. The Mt. Etna plumbing system: The contribution of seismic tomography. In: Bonaccorso, A, et al. (Eds.), Etna Volcano Laboratory. Geophys. Monogr. Ser., vol. 143, , AGU, Washington, D. C., pp. 191– 204.

Cocco, M., Rice, J., 2002. Pore pressure and poroelasticity effects in Coulomb stress analysis of earthquake interactions. J. Geophys. Res. 107. doi:10.1029/2000JB000138.

Corsaro, R.~~-~~A., Pompilio, M., 2004. Dynamics of magmas at Mount Etna. In: Bonaccorso, A, et al. (Eds.), Etna Volcano Laboratory. Geophys. Monogr. Ser., vol. 143, ~~,~~ AGU, Washington, D. C., pp. 91– 110.

Corsaro, R.~~-~~A., Civetta, L., Di Renzo, B., Miraglia, L., 2009. Petrology of lavas from the 2004-2005 flank eruption of Mt. Etna, Italy: inferences on the dynamics of magma in the shallow plumbing sysyem. Bull. Volcanol. 71, 781-793,~~.~~ doi:10.1007/s00445-009-0264-z.

Comninou, M. A., Dundurs, J., 1975. The angular dislocation in a half-space. J. Elasticity 5, 203–216.

Crouch, S.~~–~~L., Starfield, A.~~–~~M., 1983. Boundary Element Methods in Solid Mechanics: With Applications in Rock Mechanics and Geological Engineering. Allen and Unwin, St. Leonards, N.S.W., Australia.

Currenti, G., Del Negro, C., Ganci, G., Williams, C. A., 2008., Static stress changes induced by the magmatic intrusions during the 2002–2003 Etna eruption. J. Geophys. Res. 113, B10206, doi:10.1029/2007JB005301.

Currenti, G., Bonaccorso, A., Del Negro, C., Scandura, D., Boschi, E., 2010. Elasto-plastic modeling of volcano ground deformation. Earth and Planetary Science Letters 296, 311–318.

Gardunõ, V.~~-~~H., ~~M.~~ Neri, M., ~~G.~~ Pasquarè, G., ~~A.~~ Borgia, A.,~~and A.~~ Tibaldi, A., ~~(~~1997~~)~~.~~,~~ Geology of NE-Rift of Mount Etna, Sicily (Italy)~~,~~. Acta Vulcanol.~~,~~ 9(1/2), 91– 100.

Gresta, S., Longo, V., Viavattene, A., 1990. Geodynamic behaviour of eastern and western sides of Mt. Etna. Tectonophysics 179, 81 – 92. doi:10.1016/0040-1951(90)90357-E.

Gresta, S., Ghisetti, F., Privitera, E., Bonanno A., 2005. Coupling of eruptions and earthquakes at Mt. Etna (Sicily, Italy): A case study from the 1981 and 2001 events. Geophys. Res. Lett. 32. doi:10.1029/ 2004GL021479.

Harris, R.~~-~~A., 1998. Introduction to special section: Stress triggers, stress shadows, and implications for seismic hazard. J. Geophys. Res. 103, 347–24.

Hill, D.P., Pollitz, F., Newhall, C., 2002. Earthquake-volcano interactions Phys. Today 55(11), 41–47.

King, G.C.P., Stein, R.S., Lin, J., 1994. Static stress changes and the triggering of earthquakes Bull. Seismol. Soc. Am. 84, 935– 953.

King, G.C.P., Cocco, M., 2000). Fault interaction by elastic stress changes: new clues from earthquake sequences. Adv. Geophys.44, 1–38.

Lentini, F., 1982. The geology of the Mt. Etna basement. Mem. Soc. Geol. Ital. 23, 7 –25.

Lo Giudice, E., Rasà, R., 1992 Very shallow earthquakes and brittle deformation in active volcanic areas: The Etnean region as an example. Tectonophysics 202, 257– 268.

Maerten, F., Resor, P., Pollard, D., Maerten, L., 2005. Inverting for slip on three-dimensional fault surfaces using angular dislocations. Bull. Seism. Soc. Am. 95, 1654–1665. doi:10.1785/0120030181

McGuire, W.J., 1996 Volcano instability: A reviewof contemporary themes. In: McGuire, W.M., Jones, A.P., Neuberg, J., (Eds.), Volcano Instability on the Earth and Other Planets. Geol. Soc. Spec. Publ., Geological Society (London) Special Publications 110, pp. 1– 23.

~~Merle, O., Borgia, A., 1996. Scaled experiments of volcanic spreading, J. Geophys. Res. 101, 13805–13817.~~

Monaco, C., Catalano, S., Cocina, O., De Guidi, G., Ferlito, C., Gresta, S., Musumeci, C., Tortorici, L., 2005. Tectonic control on the eruptive dynamics at Mt. Etna volcano (eastern Sicily) during the 2001 and 2002-2003 eruptions. *J. Volcanol. Geotherm. Res*. 144, 211-233.

Montalto, A., Vinciguerra, S., Menza, S., Patanè, G., 1996. Recent seismicity of Mount Etna: implications for flank instability, In: McGuire, W.J., Jones, A.P., Neuberg, J., (Eds.), Volcano instability on the Earth and other planets. Geological Society (London) Special Publications 110, pp. 169-177.

Neri, M., Gardunõ, V.-H., Pasquarè, G., Rasà, R., 1991. Studio strutturale e modello cinematico della Valle del Bove e del settore nord-orientale etneo. Acta Vulcanol. 1, 17– 24. (in Italian)

Neri, M., Mazzarini, F., Tarquini, S., Bisson, M., Isola, I., Behncke, B., Pareschi, M.T., 2008. The changing face of Mount Etna's summit area documented with Lidar technology Geophys. Res. Lett. 35,. doi:10.1029/2008GL033740.

Nostro, C., Stein, R.S., Cocco, M., Belardinelli, M.-E., Marzocchi, W., 1998. Two-way coupling between Vesuvius eruptions and southern Apennine earthquakes, Italy, by elastic stress transfer. J. Geophys. Res. 103, 24487– 24504.

Patanè, D., De Gori, P., Chiarabba, C., Bonaccorso, A., 2003a. Magma ascent and the pressurization of Mount Etna's volcanic system. Science 299, 2061– 2063.

Patanè, D., Privitera, E., Gresta, S., Akinci, A., Alparone, S., Barberi, G., Chiaraluce, L., Cocina, O., D'Amico, S., De Gori, P., Di Grazia, G., Falsaperla, S., Ferrari, F., Gambino, S., Giampiccolo, E., Langer, H., Maiolino, E., Moretti, M., Mostaccio, A., Musumeci, C., Piccinini, D., Reitano, D.,

Formatted: Italian (Italy)

Scarfì, L., Spampinato, S., Ursino, A., Zuccarello, L., 2003b. Seismological constrains for the dike emplacement of the July-August 2001 lateral eruption at Mt. Etna volcano, Italy. *Ann. Geophys*. 46, 599-608.

Patanè, D., Barberi, G., Cocina, O., De Gori, P., Chiarabba, C., 2006. Time-resolved seismic tomography detects magma intrusions at Mount Etna, Science 313**,** 821–823.

Palano, M., Puglisi, G., Gresta, S., 2007. Ground deformation at Mt. Etna: a joint interpretation of GPS and InSAR data from 1993 to 2000. Boll. Geofis. Teor. Appl. 48, 81–98.

~~Palano, M., Puglisi, G., Gresta, S., 2008. Ground deformation patterns at Mt. Etna from 1993 to 2000 from joint use of InSAR and GPS techniques. J. Volcanol. Geotherm. Res. 169, 99-120. doi:10.1016/j.jvolgeores.2007.08.014.~~

Palano, M., Gresta, S., Puglisi, G., 2009. Time-dependent deformation of the eastern flank of Mt. Etna: after-slip or viscoelastic relaxation? Tectonophysics 473, 300-311. doi:10.1016/j.tecto.2009.02.047.

Puglisi, G., Bonforte, A., ~~(~~2004~~),~~. Dynamics of Mount Etna Volcano inferred from static and kinematic GPS measurements.~~,~~ J. Geophys. Res.~~,~~ 109, B11404, doi:10.1029/2003JB002878.

Puglisi, G., Bonforte, A., Ferretti, A., Guglielmino, F., Palano, M., Prati, C., 2008. Dynamics of Mount Etna before, during, and after the July–August 2001 eruption inferred from GPS and differential synthetic aperture radar interferometry data. J. Geophys. Res. 113. doi:10.1029/2006JB004811.

Rasà, R., Azzaro, R., Leonardi, O., 1996. Aseismic creep on faults and flank instability at Mt. Etna volcano. In: McGuire, W.J., Jones, A.P., Neuberg, J., (Eds.), Volcano instability on the Earth and other planets. Geological Society (London) Special Publications 110, pp. 179– 192.

Reasenberg, P.A., Simpson, R.W., 1992. Response of regional seismicity to the static stress change produced by the Loma Prieta earthquake. Science 255, 1687-1690.

Saraò, A., Cocina, O., Privitera, E., Panza, G.-F., 2010. The dynamics of the 2001 Etna eruption as seen by full moment tensor analysis. Geophys. J. Int. 181, 951–965. doi:10.1111/j.1365-246X.2010.04547.x.

Savage, J.C., Clark, M.M., 1982. Magmatic resurgence in the long valley caldera, California: possible cause of the 1980 Mammoth Lakes earthquakes. Science 217**,** 531–533.

~~Segall, P., Desmarais, E., Shelly, D., Miklius, A., Cervelli, P., 2006. Earthquakes triggered by silent slip events on Kilauea Volcano, Hawaii. Nature 442. doi:10.1038/nature04938.~~

~~Siebert, L., 1984. Large volcanic debris avalanches – characteristics of source areas, deposits, and associated eruptions. J. Volc. Geotherm. Res. 163-197. Doi:10.1016/0377-0273(84)90002-7.~~

Stein, R. S., 1999. The role of stress transfer in earthquake occurrence. Nature 402, 605–609.

Tarquini, S., Isola, I., Favalli, M., Mazzarini, F., Bisson, M., Pareschi, M.T., Boschi, E., 2007. TINITALY/01: a new Triangular Irregular Network of Italy. Annals of Geophysics 50, 3, 407- 425.

Thomas, A.-L., 1993. Poly3D: A three-dimensional, polygonal element, displacement discontinuity boundary element computer program with applications to fractures, faults, and cavities in the Earth's crust. M. S. thesis, Stanford University, Stanford, California – U.S.A.

Tibaldi, A., 2001. Multiple sector collapses at Stromboli volcano, Italy: How they work. Bull. Volcanol. 63, 112–125.

Tibaldi, A., Groppelli, G., 2002. Volcano-tectonic activity along structures of the unstable NE flank of Mount Etna (Italy) and their possible origin. J. Volcanol. Geotherm. Res. 115, 277– 302.

Toda, S., Stein, R.S., Sagiya, T., 2002. Evidence from the AD 2000 Izu Islands earthquake swarm that stressing rate governs seismicity. Nature 419, 58–61.

Voight, B., Elsworth, D., 1992. Resolution of mechanics problems for prodigious Hawaiian landslides: Magmatic intrusions simultaneously increase driving force and reduce driving resistance by fluid pressure enhancement. *Eos Transactions* 73(43), AGU Fall Meeting suppl., 506.

Voight, B., Elsworth, D., 1997. Failure of volcano slopes. Geotechnique 47, 1 – 31.

Walter, T.-R., Acocella, V., Neri, M., Amelung F., 2005. Feedback processes between magmatic events and flank movement at Mount Etna (Italy) during the 2002–2003 eruption. J. Geophys. Res. 110. doi:10.1029/2005JB003688.

Figure captions

Figure 1. Structural sketch map of ~~Mt.~~Mount Etna: Provenzana Fault (PR); Pernicana fault (PF); Santa Venerina fault (SVF); Timpe fault system STF; Moscarello fault (MF); Tremestieri–Trecastagni fault (TTF); San Leonardello Fault (SLF); Central Craters (CC); South Rift and North - East Rift are also indicated. In the upper inset, the location of ~~Mt.~~Mount Etna in the central Mediterranean area and a simplified geological map of eastern Sicily are also reported. The INGV-G-DEM is in the WGS84 reference system and the projection is UTM33.

Figure 2. a) Top view and b) prospective view of the boundary Element model built in Poly3D environment show spatial relationships between topography, faults, magmatic reservoir, eruptive fractures, sliding plane and faults. For structure legend see tables 1 and 2.

Figure 3. Sketch of four models proposed showing: M1) Inflation of Magmatic Reservoir (MR); M2A) Opening of South Dike (SD); M2B) Opening of North-East Dike (NED); M3) Transtensive movement of Sliding Plane (SP); the acting sources ~~acting~~ (red) and the receiver structures (black) are drawn. For faults legend see table 2.

Figure 4. Three dimensional view showing the pattern of ΔCFS produced by inflation of MR (M1) along modeled fault planes; Opening of SD (M2A); Opening of NED (M2B) and Transtensive movement of SP (M3). The color bar specifies ~~only~~ the ~~relative~~ maximum and minimum ΔCFS values~~.~~ that are reported for ~~These values calculated for~~ each single ~~plane~~ structure ~~are reported~~ in Tables 3-6.

Figure 5. Three dimensional view showing the pattern of the displacement produced by inflation of MR (M1) along modeled fault planes; Opening of SD (M2A); Opening of NED (M2B) and Transtensive movement of SP (M3). The color bar specifies the maximum and minimum displacement values that are reported for each single structure in Tables 3-6. The color bar specifies only the relative maximum and minimum displacement values. The maximum displacement values calculated for each single plane are reported in Tables 3-6.

Table titles

Table 1. Description of deformation source inputs used in the numerical modeling. Xc, Yc and Zc represent the location of the center, while L and W correspond to length and width for each source.

Table 2. Position and geometrical parameters of receiver fault planes modeled in Poly3D program (for symbols explanation see table 1).

Table 3. Coulomb stress changes and displacements (U) induced on considered structures (see table 1 and 2 for structure names) by the inflation of MR (model M1).

Table 4. Coulomb stress changes and displacements (U) induced on considered structures (see table 1 and 2 for structure names) by the opening of SD (model M2A).

Table 5. Coulomb stress changes and displacements (U) induced on considered structures (see table 1 and 2 for structure names) by the opening of NED (model M2B).

Table 6. Coulomb stress changes and displacements (U) induced on considered structures (see table 1 and 2 for structure names) by the transtensive movement of SP (model M3).

Table 1
Click here to download Table: Table 1.docx

Table 1

Name	Source	Xc (m)	Yc (m)	Zc (m)	L (m)	W (m)	Dip (°)	Dislocation (m)	N° nodes	N° elements
NED	Northeastern Dike	501518.5	4181600	960.4715	5956	3914	90	Opening 2.5	511	893
SD	Southern Dike	500053	4175720	1071.465	3132	3022	90	Opening 2.5	691	1234
SP	Sliding Plane	517526	4170940	-2997.11	20000	25000	11	Left Lateral 0.077 Normal slip 0.042	6519	12736
MR	Magmatic Reservoir	499593	4177480	-2900	R = 1000			∆V 7.9*10e6	815	1624

Table 2
Click here to download Table: Table 2.docx

Table 2

Name	Tectonic Lineament	Xc	Yc	Zc	L	W	Dip	N° Nodes	N° Elements
PR	Provenzana Fault	503089	4183165	492	2326	4000	87	473	830
PF1	Pernicana Segment 1	506317	4184280	311	4972	4000	87	703	1241
PF2	Pernicana Segment 2	510575	4183870	-9	3465	4000	87	583	1049
PF3	Pernicana Segment 3	513277	4182470	-131	4582	4000	87	572	1015
PF4	Pernicana Segment 4	516913.5	4180680	-418	2962	4000	87	495	873
STF1	S. Tecla Fault 1	512725.5	4168130	-1065	7602	1948	87	353	624
STF2	S. Tecla Fault 2	515354.5	4162020	-1376	6252	2809	87	342	610
SVF	S.Venerina Fault	512891	4169375	-1013	5556	2577	87	313	536
SLF	S.Leonardello Fault	515289.5	4170575	-1302	9040	2788	87	304	513
MF	Moscarello Fault	513805	4170660	-1074	11190	2664	87	231	374
TTF	Tremestieri - Trecastagni Fault	508857.5	4159625	-1265	6377	3252	87	340	1227

Table 3
Click here to download Table: Table 3.docx

Table 3

	Coulomb (bars)		Stress Component (bars)		U (cm)	
	min	max	Shear	Normal	min	max
PR	-3.0	-1.0	-1.4	-0.4	1.6	3.0
PF1	0.3	1.4	0.7	0.0	0.9	2.0
PF2	-0.5	-0.2	-0.4	0.0	0.6	1.1
PF3	0.0	0.2	0.2	-0.2	0.5	0.9
PF4	-0.2	-0.1	-0.1	-0.1	0.4	0.6
STF1	0.1	0.3	0.2	0.1	0.4	0.9
STF2	-0.1	-0.1	0.0	-0.1	0.3	0.4
SVF	0.1	0.2	0.1	0.3	0.4	0.9
SLF	-0.1	0.1	-0.1	0.2	0.3	0.7
MF	0.0	0.2	0.1	0.2	0.4	0.9
TTF	0.1	0.2	0.1	0.0	0.3	0.5
SP	-1.9	0.2	0.0	-0.1	0.1	2.4
SD	-20.7	-0.2	$\Delta\sigma$(bars)		4.7	12.7
NED	-8.3	0.4	$\Delta\sigma$(bars)		1.9	12.7

Table 4

	Coulomb (bars)		Stress Component (bars)		U (cm)	
	min	max	Shear	Normal	min	max
PR	-4.5	-0.8	-3.1	-1.2	2.2	3.9
PF1	-0.7	1.4	1.4	2.4	2.1	3.8
PF2	-1.2	0.1	0.7	2.8	3.0	3.8
PF3	-0.7	0.4	-0.4	-0.5	2.8	3.7
PF4	0.3	0.7	0.4	-0.2	2.3	3.0
STF1	-2.2	-0.3	-1.0	0.4	0.9	3.8
STF2	-0.4	-0.2	-0.3	-0.1	0.4	1.2
SVF	-2.1	-0.5	-1.2	0.3	1.3	3.8
SLF	-0.3	0.7	-0.2	1.5	1.0	3.8
MF	0.3	1.6	0.3	1.8	0.9	4.9
TTF	-0.2	-0.1	-0.1	-0.1	0.4	0.7
SP	-8.8	2.6	-0.5	0.3	0.4	11.5
MR	-6.42E-05	1464.33	$\Delta\varepsilon$		6.9	33.1
NED	-32.4	-0.1	$\Delta\sigma$ (bars)		2.1	9.9

Table 5

	Coulomb (bars)		Stress Component (bars)		U (cm)	
	min	max	Shear	Normal	min	max
PR	-135.0	323.5	38.9	120.6	16.4	130.1
PF1	6.3	102.2	20.8	-13.5	5.8	19.9
PF2	1.9	3.4	4.4	3.9	5.1	8.0
PF3	-2.9	-0.7	-2.7	-1.3	5.0	7.3
PF4	0.0	0.7	-0.1	-1.0	4.2	5.5
STF1	-2.0	-0.5	-1.8	2.1	3.1	7.7
STF2	-0.9	-0.4	-0.7	0.1	1.9	3.5
SVF	-2.4	-0.7	-2.2	2.1	3.7	7.8
SLF	1.2	2.3	3.3	0.5	3.2	7.7
MF	1.3	5.3	1.8	3.3	3.1	9.8
TTF	-0.5	-0.2	-0.6	0.6	1.5	2.4
SP	-18.5	5.7	-1.2	1.7	1.3	24.8
MR	-4.88E-05	-1.5E-5	$\Delta\varepsilon$		8.9	15.6
SD	-25.9	-3.7	$\Delta\sigma$ (bars)		5.5	13.3

Table 6

	Coulomb (bars)		Stress Component (bars)		U (cm)	
	min	max	Shear	Normal	min	max
PR	-0.5	0.1	-0.1	0.1	0.6	9.3
PF1	-0.7	1.7	0.6	-0.6	0.6	9.0
PF2	-0.2	1.5	0.9	-0.3	1.1	2.3
PF3	0.3	1.0	-0.7	-2.9	1.5	3.1
PF4	1.3	3.5	1.2	-2.1	3.0	3.5
STF1	-0.2	0.2	-0.2	0.4	3.8	5.5
STF2	-24.9	0.0	-1.4	0.5	0.8	5.2
SVF	-0.2	0.2	-0.1	0.4	4.2	5.5
SLF	-0.1	0.6	0.0	0.5	4.0	5.4
MF	-0.2	0.7	0.1	0.3	3.9	5.5
TTF	-4.7	3.1	-0.2	0.1	0.3	8.9
MR	1.97E-07	6.5E-7	$\Delta\varepsilon$		0.5	0.9
Sdike	-0.9	0.2	$\Delta\sigma$ (bars)		0.5	1.2
NEdike	-0.8	0.1	$\Delta\sigma$ (bars)		0.4	8.9

1

Figure 1

Click here to download high resolution image

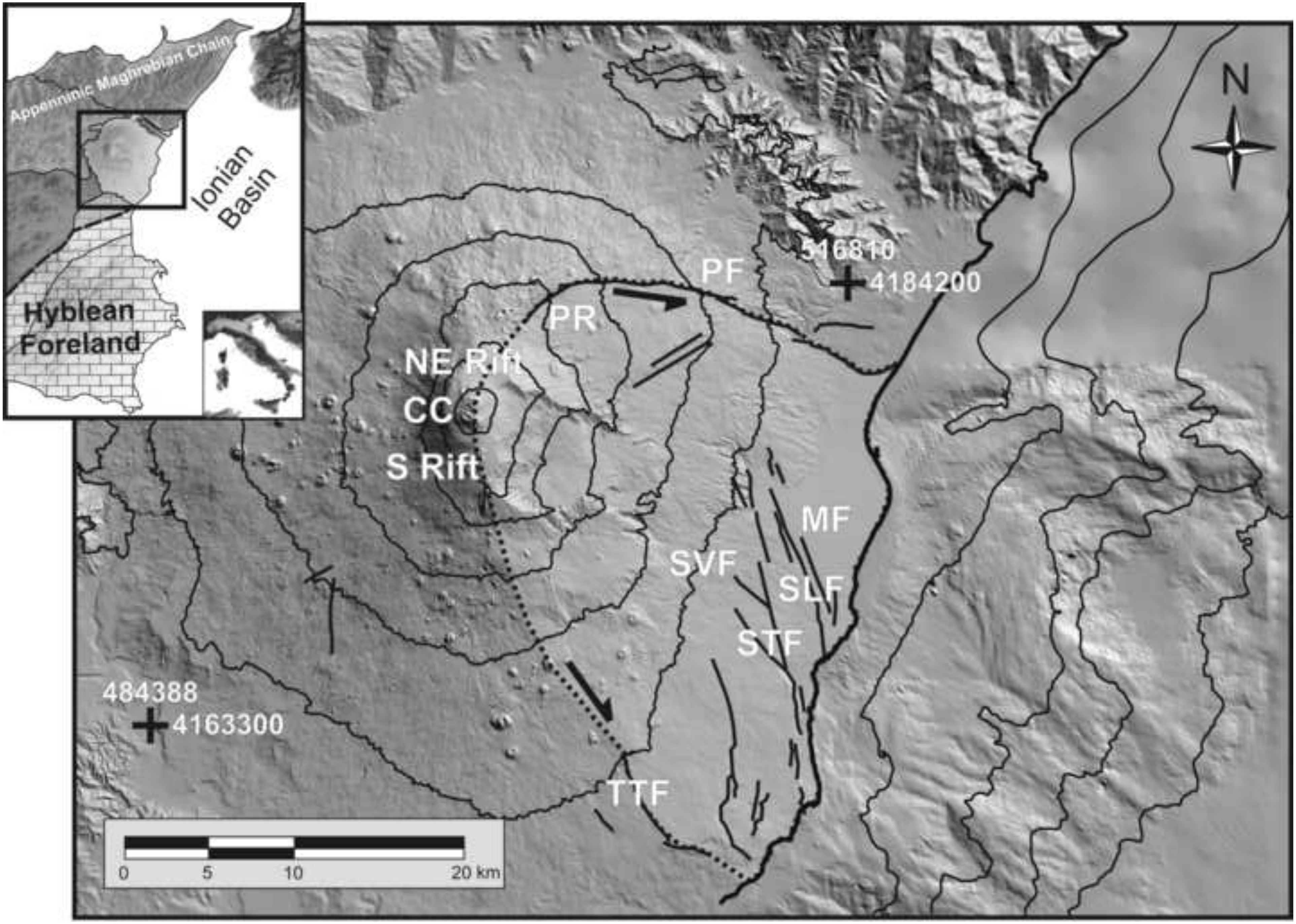

Figure 2
Click here to download high resolution image

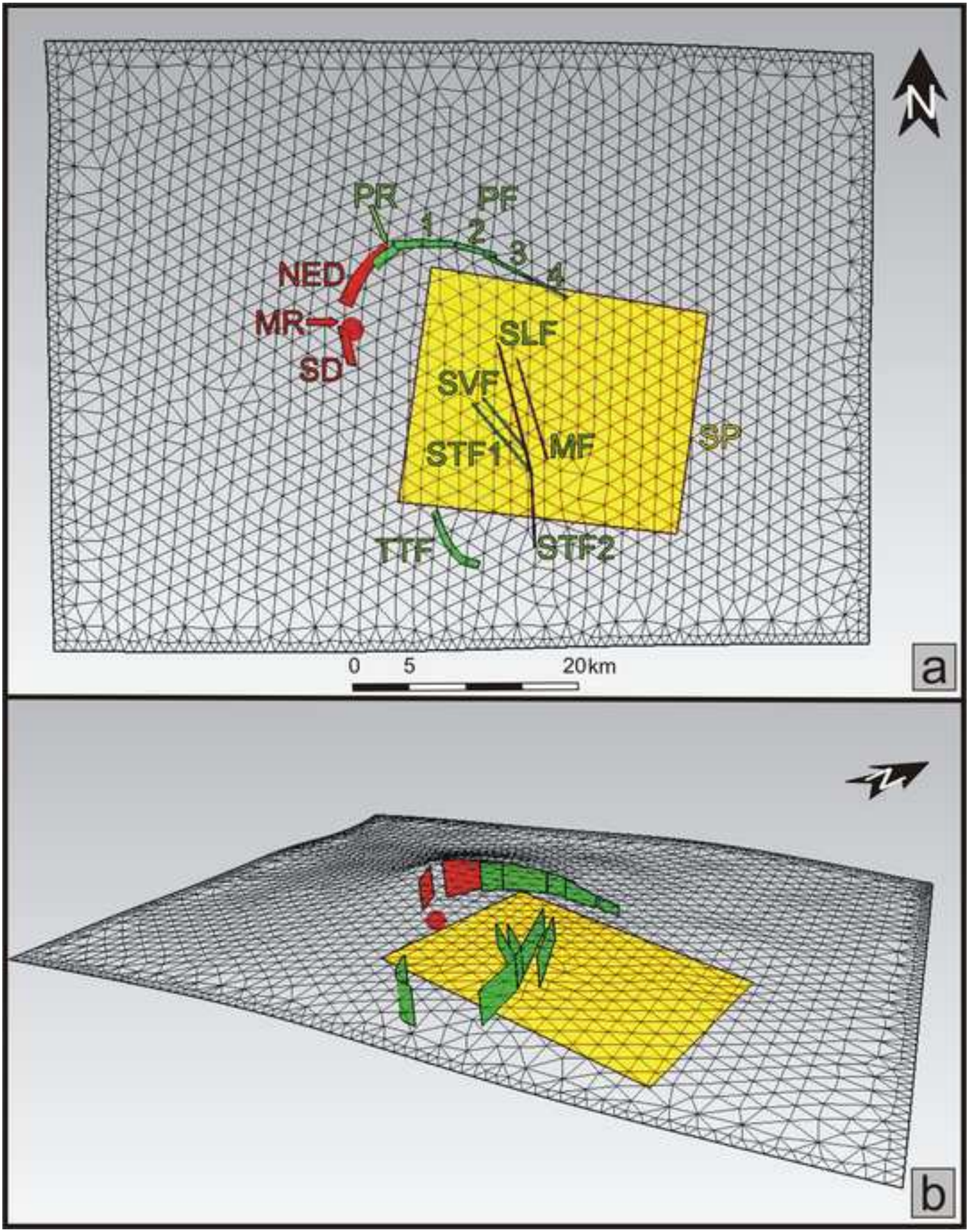

Figure 3
Click here to download high resolution image

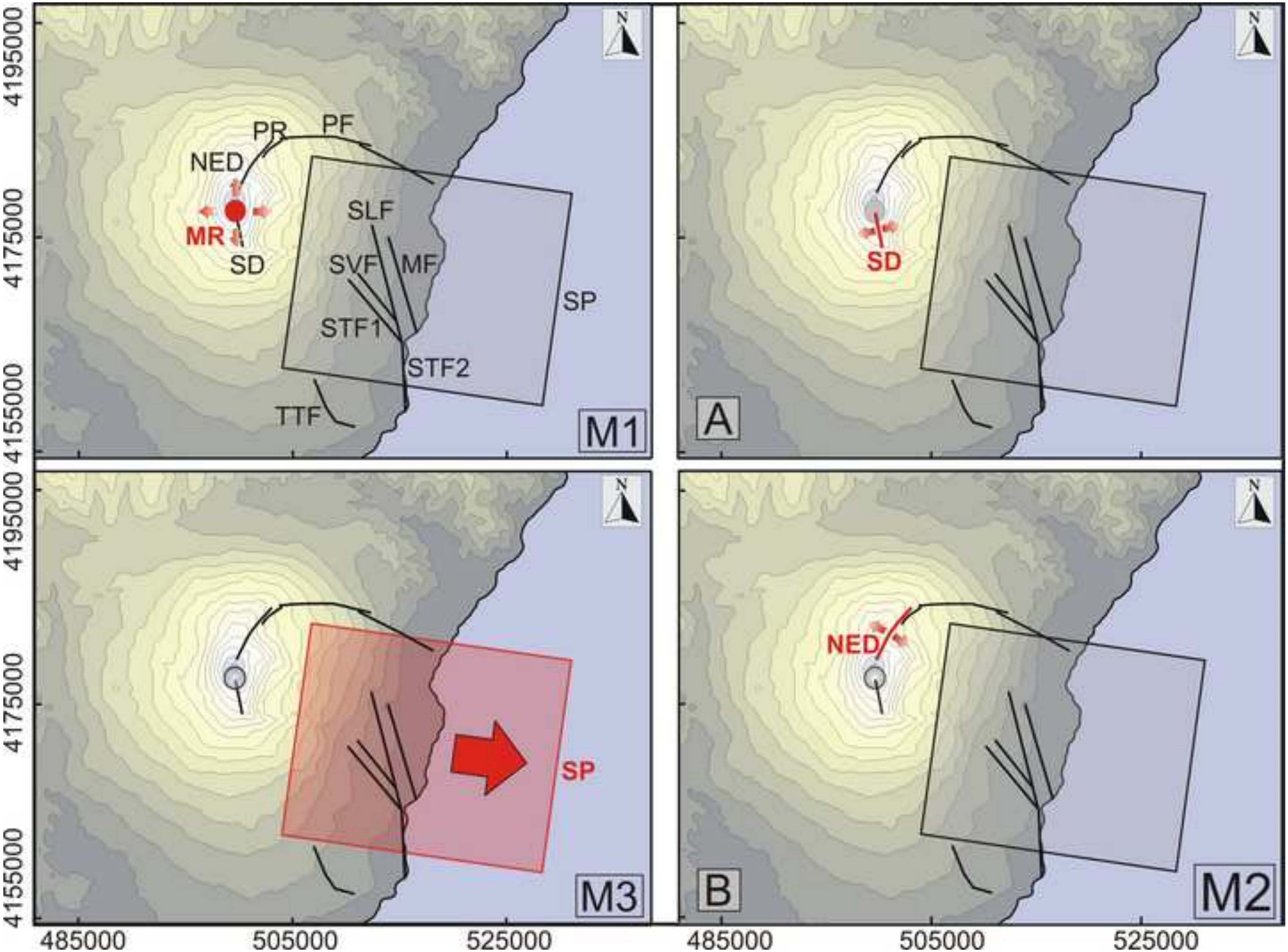

Figure 4
Click here to download high resolution image

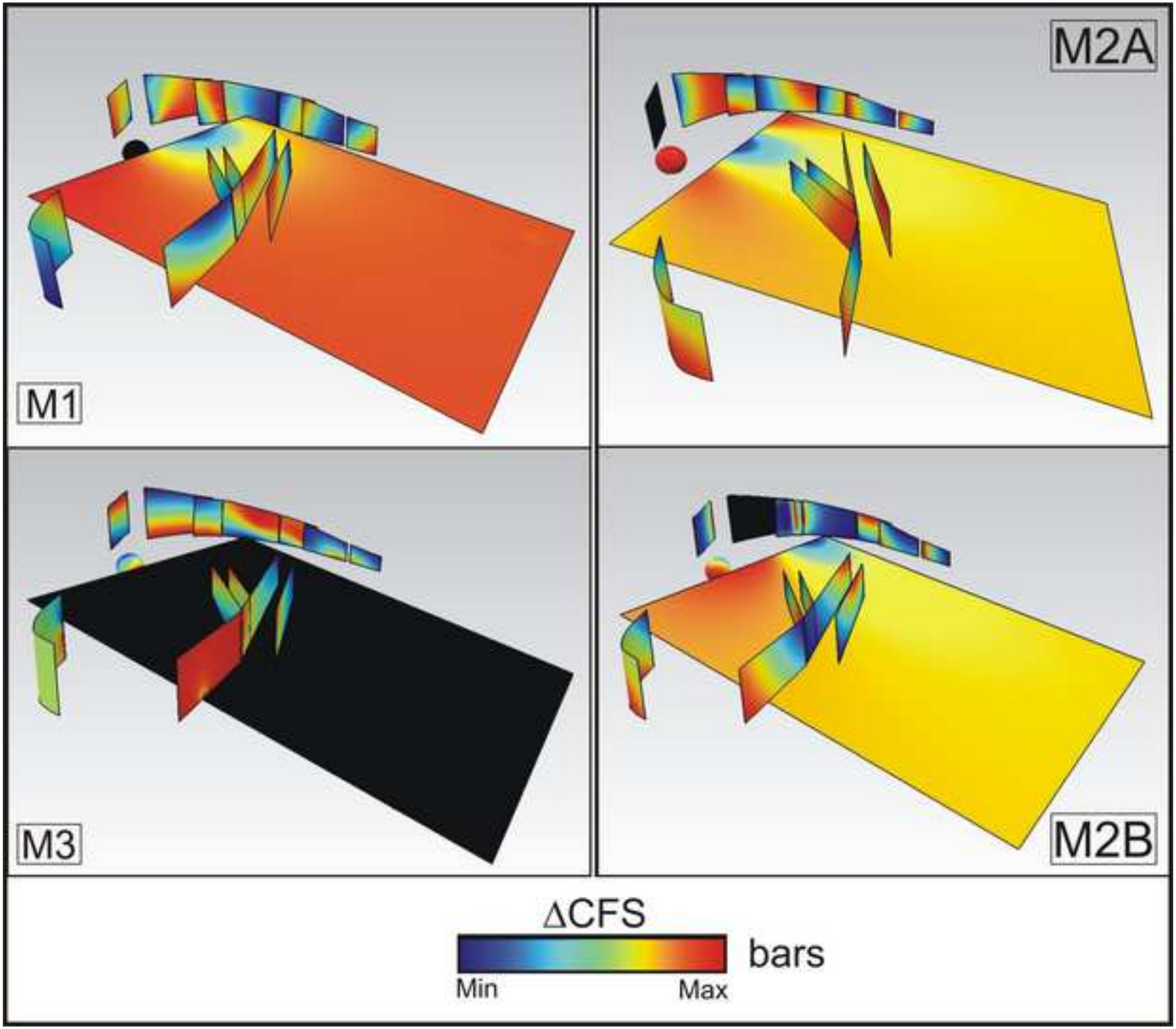

Figure 5
Click here to download high resolution image